AGU Advances

Second Revision of

The Chicxulub Impact Produced a Powerful Global Tsunami

Molly M. Range[1*], Brian K. Arbic[1,2], Brandon C. Johnson[3,4], Theodore C. Moore[1], Vasily Titov[5], Alistair J. Adcroft[6], Joseph K. Ansong[1,7], Christopher J. Hollis[8], Jeroen Ritsema[1], Christopher R. Scotese[9], and He Wang[1,10,11]

[1] Department of Earth and Environmental Sciences, University of Michigan, Ann Arbor, MI 48109, USA
[2] Recently on sabbatical at Institut des Géosciences de L'Environnement (IGE), Grenoble, France, and Laboratoire des Etudes en Géophysique et Océanographie Spatiale (LEGOS), Toulouse, France
[3] Department of Earth, Atmospheric, and Planetary Sciences, Purdue University, West Lafayette, IN 47907, USA
[4] Department of Physics and Astronomy, Purdue University, West Lafayette, IN 47907, USA
[5] National Oceanic and Atmospheric Administration, Pacific Marine Environmental Lab, Seattle, WA 98155, USA
[6] Atmospheric and Oceanic Sciences Program, Princeton University, Princeton, NJ 08540, USA
[7] Department of Mathematics, University of Ghana, P.O. Box LG 62, Legon, Accra, Ghana
[8] School of Geography, Environment and Earth Sciences, victoria University of Wellington, New Zealand
[9] PALEOMAP Project, 134 Dodge, Evanston, IL 60202, USA
[10] Oceanic and Atmospheric Administration, Geophysical Fluid Dynamics Laboratory, Princeton, NJ 08540, USA
[11] University Corporation for Atmospheric Research, P.O. Box 3000, Boulder, CO 80307-3000

The Chicxulub Impact Produced a Powerful Global Tsunami

Molly M. Range[*1], Brian K. Arbic[1,2], Brandon C. Johnson[3,4], Theodore C. Moore[1], Vasily Titov[5], Alistair J. Adcroft[6], Joseph K. Ansong[1,7], Christopher J. Hollis[8], Jeroen Ritsema[1], Christopher R. Scotese[9], and He Wang[1,10,11]

[1]Department of Earth and Environmental Sciences, University of Michigan, Ann Arbor, MI, 48109, USA; [2]Recently on sabbatical at Institut des Géosciences de L'Environnement (IGE), Grenoble, France, and Laboratoire des Etudes en Géophysique et Océanographie Spatiale (LEGOS), Toulouse, France; [3]Department of Earth, Atmospheric, and Planetary Sciences, Purdue University, West Lafayette, IN 47907, USA; [4]Department of Physics and Astronomy, Purdue University, West Lafayette, IN 47907, USA; [5]National Oceanic and Atmospheric Administration, Pacific Marine Environmental Lab, Seattle, WA 98155, USA; [6]Atmospheric and Oceanic Sciences Program, Princeton University, Princeton, NJ 08540, USA; [7]Department of Mathematics, University of Ghana, P.O. Box LG 62, Legon, Accra, Ghana; [8]School of Geography, Environment and Earth Sciences, Victoria University of Wellington, New Zealand;[9]PALEOMAP Project, 134 Dodge, Evanston, IL 60202, USA; [10]National Oceanic and Atmospheric Administration, Geophysical Fluid Dynamics Laboratory, Princeton, NJ 08540, USA; [11]University Corporation for Atmospheric Research, P.O. Box 3000, Boulder, CO, 80307-3000

Corresponding author: Molly Range (mmrange@umich.edu)

Key Points:

- The authors present the first global simulation of the Chicxulub impact tsunami
- Total energy present in the impact tsunami is much greater than for any modern-day tsunami
- Impact tsunami flow velocities are strong enough to disturb and erode sediment in basins halfway around the globe

Abstract

The Chicxulub crater is the site of an asteroid impact linked with the Cretaceous-Paleogene (K-Pg) mass extinction at ~66Ma. This asteroid struck in shallow water and caused a large tsunami. Here we present the first global simulation of the Chicxulub impact tsunami from initial contact of the projectile to global propagation. We use a hydrocode to model the displacement of water, sediment, and crust over the first ten minutes, and a shallow-water ocean model from that point onwards. The impact tsunami was up to 30,000 times more energetic than the December 26, 2004 Indian Ocean tsunami, one of the largest tsunamis in the modern record. Flow velocities exceeded 20 cm/s along shorelines worldwide, as well as in open-ocean regions in the North Atlantic, equatorial South Atlantic, southern Pacific and the Central American Seaway, and therefore likely scoured the seafloor and disturbed sediments over 10,000 km from the impact origin. The distribution of erosion and hiatuses in the uppermost Cretaceous marine sediments are consistent with model results.

Plain Language Summary

At the end of the Cretaceous, about 66 million years ago, the Chicxulub asteroid impact near the Yucatan peninsula produced a global tsunami 30,000 times more energetic than any modern-day tsunami produced by earthquakes. Here we model the first ten minutes of the event with a crater impact model, and the subsequent propagation throughout the world oceans using two different global tsunami models. The Chicxulub tsunami approached most coastlines of the North Atlantic and South Pacific with waves of over

10 meters high and flow velocities in excess of 1 m/s offshore. The tsunami was strong enough to scour the seafloor in these regions, thus removing the sedimentary records of conditions before and during this cataclysmic event in earth history and leaving either a gap in these records or a jumble of highly disturbed older sediments. The gaps in sedimentary records generally occur in basins where the numerical model predicts larger bottom velocities.

1 Introduction

The impact of an approximately 14-km diameter asteroid is implicated in the Cretaceous/Paleogene (K-Pg) mass extinction (Schulte et al., 2010) approximately 66 Ma ago. The bolide impact caused global temperature fluctuations (Schulte et al., 2010), large aerosol plumes (Bardeen et al., 2017), large plumes of soot and dust (Brugger et al., 2017), wildfires from ejecta re-entering the atmosphere (Busby et al., 2002; Morgan et al., 2013), and a massive tsunami (Matsui et al., 2002; Kinsland et al., 2021). Drilling cores from the Integrated Ocean Drilling Program (Gulick et al., 2016) and the International Continental Drilling Program (ICDP) corroborated the models (Collins et al., 2008) of the exact physical and geophysical nature of the crater and its peak ring which has facilitated detailed modeling of the impact (Morgan et al., 2016). Earlier tsunami simulations described the effects of the tsunami within the confines of the Gulf of Mexico (e.g., Ward, 2012; Matsui et al., 2002; see Ward, 2021 for a more recent simulation extending beyond the Gulf of Mexico). Subsequent submarine landslides on the marine shelf (Gulick et al., 2008) could potentially increase the energy of this tsunami.

Most global tsunami simulations to date have been of tsunamis induced by underwater earthquakes, for instance, the 2004 Indian Ocean tsunami (Smith et al., 2005, Titov et al., 2005). Tsunami propagation has traditionally been simulated with shallow-water ocean models, which assume hydrostatic water pressure and a small depth-to-wavelength ratio. Such models cannot be used to simulate the complex first ten minutes of the Chicxulub impact tsunami when there was large-scale deformation of the crust and the formation of a crater (Morgan et al., 2016). The crater formation and post-impact ejecta splashing back into the ocean create highly non-linear and non-hydrostatic waves. Modeling the impact tsunami requires a multi-stage simulation, with hydrocode modeling of crater formation and post-impact non-hydrostatic water waves, before hand-off of the solution to global shallow-water models. We pursue such a two-stage strategy in this paper.

These linked models seek to depict a complex set of events associated with the asteroid impact and to predict the pathways of propagation as applied to a world with very different sea levels, ocean gateways, and continental positions and boundaries. The models do not incorporate a description of the chaotic near-field tectonic disturbances (e.g., faulting and slope failures) and the generation of smaller tsunamis by these disturbances. Did these aspects of the impact event alter the strength or the propagation pathway of the impact tsunami, or was this tsunami so large and so powerful that these other effects were masked and overpowered? To verify the modeled strength and pathways taken by the impact tsunami we look at a global array of K-Pg boundary intervals in marine sections on land and in ocean drilling cores. In these sites we will look for documented evidence of erosion, sediment disturbance, and/or redeposition of sediments that can be reasonably associated with the impact tsunami.

2 Impact Modeling

2.1 Methods

We use the axisymmetric iSALE-2D hydrocode (Collins et al., 2004; Wünnemann et al., 2006) to simulate the initial formation of the Chicxulub impact tsunami. iSALE-2D has been used to simulate impact-induced tsunamis (e.g., Weiss et al., 2006; Weiss and Wünnemann, 2007; Wünnemann et al., 2010). The results of our iSALE-2D simulations were used to create initial conditions for shallow-water models to trace the tsunami throughout the world's ocean.

Motivated by impact simulations that reproduce the seismically imaged structure of Chicxulub (Collins et al., 2008) as well as the peak shock pressures and composition of the basin's peak-ring, as constrained by recent drilling (Morgan et al., 2016), we assume that the 14-km-diameter impactor had a density of 2650 kg/m^3 and struck Chicxulub at 12 km/s. Although the Chicxulub impact is thought to be oblique (45-60 degrees from horizontal; Collins et al., 2020; Robertson et al., 2021) the axisymmetric nature of the code limits us to simulation of vertical impacts. We expect this limitation to have a minor effect on our results as the formation of the outward propagating rim wave (more below) is dominated by emplacement of slow ejecta that tends to be symmetric (e.g., Anderson et al., 2003). Our simulations have the same setup as those in Collins et al. (2008), but with a finer grid spacing and a larger domain needed to track the formation and early evolution of the tsunami (see SI Table 1 and other material in Supporting Information; hereafter referred to as SI). We model the target as a granitic crust overlain by a 4-km-thick layer of sediments and an ocean with a constant depth of 1, 2, or 3 km (a 2-km ocean depth was used by Collins et al. (2008) for the northwestern sector of Chicxulub). With a grid resolution of 100 m, the ocean depth is resolved by 10, 20, and 30 cells, respectively, depending on assumed ocean depths of 1, 2, and 3 km. This number of grid cells is sufficient to resolve the rim wave (Bahlburg et al., 2010; SI). The atmosphere is not expected to significantly affect the early propagation of the tsunami. Thus, we do not include the atmosphere in our simulations. Further details of the iSALE simulations used in this paper, and their sensitivities to grid spacing, can be found in SI.

2.2 Results

The dimensions and formation of the crater are similar to previous work (Collins et al., 2008; Morgan et al., 2016). The results of our "fiducial" hydrocode impact simulation, with an assumed seafloor depth of 1 km and a run time of 10 minutes, are shown in Figure 1. About 2.5 minutes after contact of the projectile, a curtain of ejecta pushing water outward from the impact produced a 4.5-km-high wave (Fig. 1a). After 5 minutes, falling ejecta continued to impart momentum to the ocean (Fig. 1b). At 10 minutes, after all the ejecta had fallen, a 1.5-km-high wave, known as a rim wave, located 220 km from the point of impact was left propagating throughout the deep ocean (Fig. 1c).

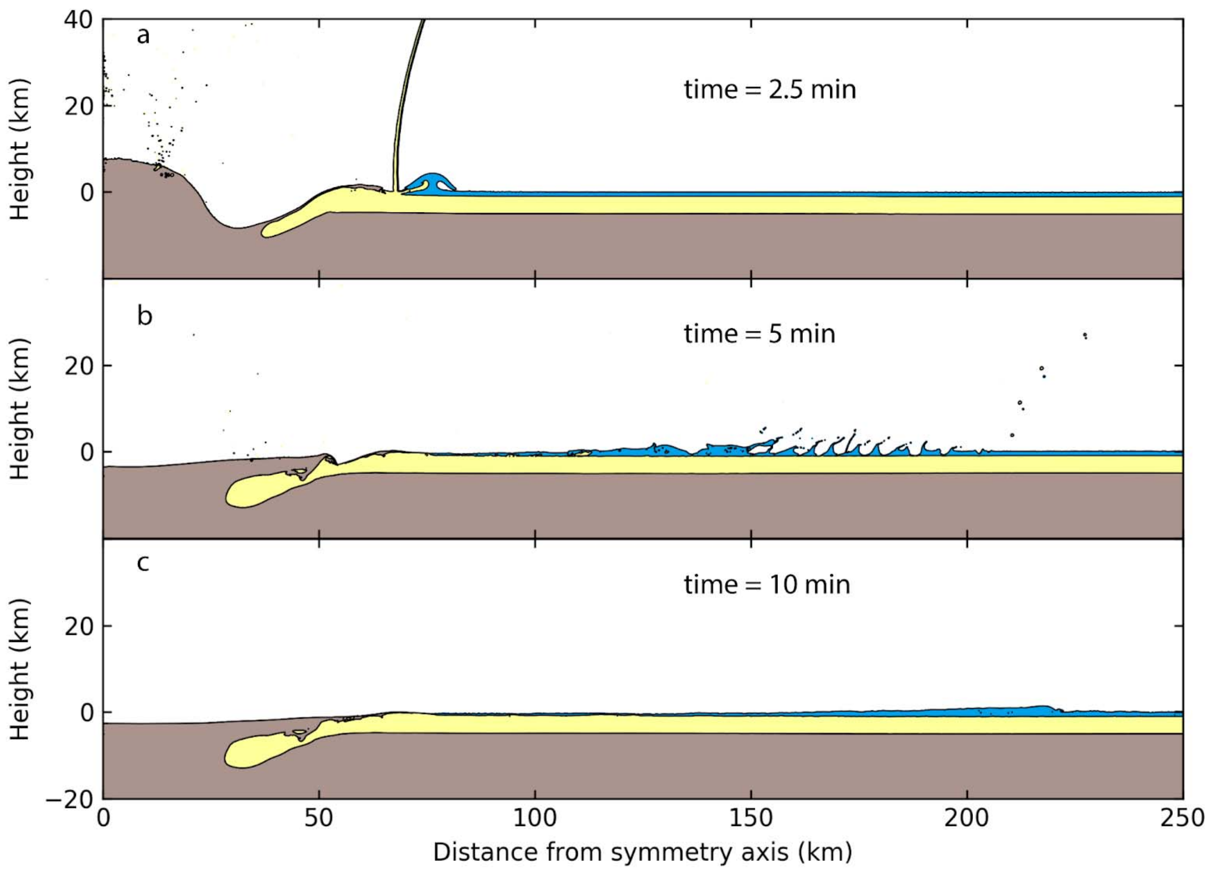

Figure 1. Formation of Chicxulub crater and the associated tsunami. Time series with material colored according to material type (crustal material is brown, sediments are yellow, and the ocean is blue). The origin marks the point of impact. Black curves mark material interfaces (e.g., sediment-crust interface). An animation of these results, from 0 to 10 minutes in steps of 5 seconds, is shown in SI Video 1.

The axisymmetric nature of our high-resolution hydrocode model requires an ocean layer with a constant water depth. The ocean depth at the point of impact is estimated to be 100-200 m (Gulick et al. 2008) and becomes deeper toward the northwest. Generation of the tsunami rim wave, however, is sensitive to the ocean depth at the crater rim, not at the point of impact. Paleobathymetry estimates indicate that water depth was ~1 km where ejecta emplacement produces the initial rim-wave (50 km from basin center). At ~150 km from the point of impact the ocean was ~3 km deep (SI Fig. 1). To test for sensitivity of the rim wave and crater shape to pre-impact ocean depth we vary the thickness of the ocean layer from 1 to 3 km. The waveforms after the first 10 minutes of the fiducial simulation, and after the first 10 minutes of iSALE simulations with different water depths, are displayed in Figure 2. These waveforms are in good agreement with the waveforms found in Bahlburg et al. (2010). SI Fig. 4 demonstrates that handoff to the MOM6 "larger mesh" results at 600 s and 850 s give nearly identical globally integrated energies. Surprisingly, the crater and rim wave structure at these early times do not depend strongly on assumed ocean depth within the range of 1-3 km (Figure 2). We do not expect this moderate dependence to hold over much deeper or shallower ocean depths. Our two-dimensional axisymmetric model with a constant depth is clearly a simplification of the bathymetry in the Gulf of Mexico. In the case of the 1 km ocean depth simulation, a sediment rim on the impact crater ten minutes into the run rose above the water column, creating a ring-shaped island. As the rim was composed of loose sediment, it would likely have been quickly dispersed by wave action (Bell et al., 2004). Other authors however have argued that resurge of water into the crater occurred by penetration through the raised rim and erosion allowing flow at locations along the rim (Bahlburg et al. 2010). To test for sensitivity to this uncertainty, we model one initial condition with a sediment rim and one without. We test for sensitivity between the two runs and found the tsunami energies to be comparable (not shown). Therefore, the 1 km water depth iSALE simulation, with no sediment rim, is used for all subsequent runs.

3 Tsunami Propagation Modeling

3.1 Methods

To simulate the global propagation of the impact tsunami, we use two different well-established shallow-water models: the Geophysical Fluid Dynamics Laboratory (GFDL) Modular Ocean Model Version 6 (Adcroft, 2017; MOM6), and Methods Of Splitting Tsunamis (Titov et al, 2016; MOST). The rim-wave has a wavelength of about 50-100 km, similar to the wavelengths seen in the 2004 Indian Ocean tsunami. As this is much greater than average ocean depths of about 4 km, the shallow water assumption, which assumes hydrostatic balance and is based on a comparison of wavelengths vs. water depth, is well satisfied. The similarity of simulations from two different models using the same underlying shallow-water approximation and run on the same 1/10th degree grid but differing in their respective numerical implementations (more below) ensures robustness of our results. Neither of the models used here explicitly include dispersive effects. Discussion of potential effects of dispersion is provided later, in the section on Future Work.

Shallow-water models solve for perturbations to the resting sea surface elevations and for depth-averaged flow velocities. Flow velocities are the velocities of particles in the water, in contrast to the phase velocities of the tsunami wave propagating throughout the ocean. The hydrostatic approximation will modify the wave speed. Errors due to this approximation are likely less than errors due to uncertainties in bathymetry. The large amplitudes of impact-generated waves lead to nonlinear dynamics during propagation, which is described only approximately by the shallow-water wave theory. Nevertheless, the long wave approximations have been successfully applied for simulating the nonlinear tsunami dynamics of propagation in shallow coastal regions and runup. Synolakis et al. (2008), for example, include an extensive discussion of verification and validation of shallow-water tsunami models with respect to field benchmarks. Their study demonstrates that large-amplitude waves can be predicted accurately with the shallow-water wave theory, providing the long wave assumption is valid. The tsunami model benchmark efforts included a wide range of depth-integrated models (Pedersen, 2008) and initiated ongoing discussion about the proper use of the shallow-water and the Boussinesq-type models for tsunami simulations (Kirby, 2016). We address the dispersive modeling issues in the "Future Work" section.

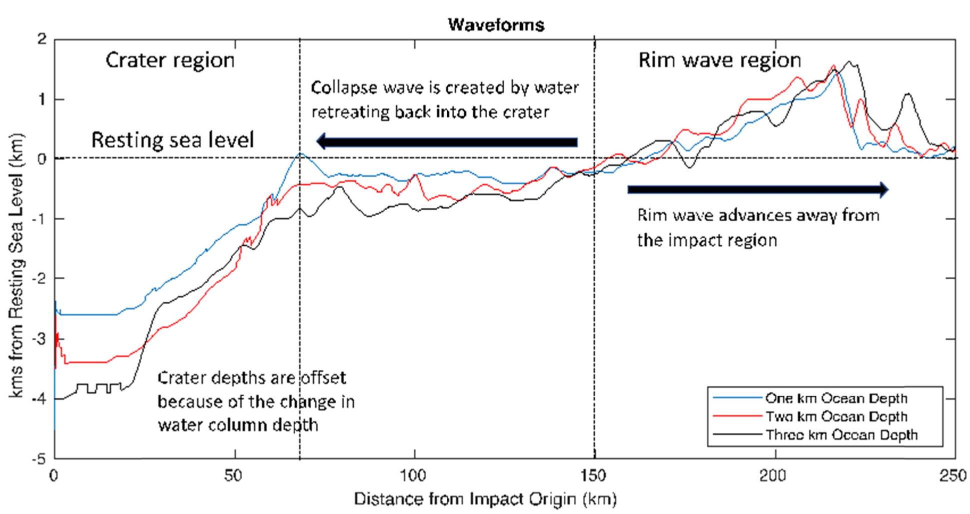

Figure 2. Waveform and crater shape for three different runs from the iSALE-2D hydrocode. In the left-most part of the plot, the crater depths are shown. The middle and right-parts of the plot follow the change

in sea level relative to the resting sea level. The crater depths are displaced by about one km from each other because of the differing ocean depths of the three runs.

MOM6 has been used to model tsunamis in the deep ocean, although it has not been used to forecast tsunamis. The barotropic solver in MOM6 is based on the solver in the Hallberg Isopycnal Model (HIM)/Generalized Ocean Layered Model (GOLD), which were used in the tsunami studies of Smith et al. (2005) and Kunkel et al. (2006). The results in Adcroft (2013) suggest that deep-ocean, large-scale motions are not overly sensitive to the horizontal resolution of the model. The "forecasting" accuracy of the tsunami calculation is not relevant for the application of the Chicxulub impact tsunami, but at $1/10^{th}$ degree global resolution the arrival times are accurate to about 1%.

MOST was developed specifically for tsunami simulations (Titov & Synolakis, 1995; Titov et al., 2016). MOST has been extensively tested for various tsunami modeling applications and has been used to simulate historical tsunamis of different origins, including modeling of global tsunami propagation and local tsunami inundation impacts. MOST is now used operationally for tsunami forecasts at NOAA Tsunami Warning Centers. While MOM6 is run for all of the cases shown in this paper, MOST is run only in the fiducial case described below.

Both tsunami propagation models used the same global $1/10^{th}$ degree bathymetric grid (SI Tables 2 and 3). To accurately simulate tsunami propagation, a global Maastrichtian (66Ma) paleobathymetry is combined with the initial condition from the hydrocode results. The sources for the global paleobathymetry are Müller et al. (2008) and Scotese (1997). More information about the bathymetries that we used, and the manner in which we combined them, can be found in SI Text S1.

To continue the simulation with the tsunami propagation codes we convert the axisymmetric, constant water depth hydrocode results (see SI Figure 2) to more realistic, non-axisymmetric conditions with horizontally varying resting water depths. The hydrocode results at 600 seconds post-impact were used for the shallow-water model initial condition. At this time there was no more resolved falling ejecta; less voluminous and potentially fine ejecta would continue to fall after 600 s, but we do not expect that this more distal ejecta would significantly affect the rim wave. At 600 s, there is a defined waveform of perturbation sea surface heights, in approximate hydrostatic balance because the wavelength is much greater than the water depth (see Fig. 2). The waveform, crater shape and velocity are isolated from the density profile. Assuming radial symmetry, the waveform is converted into a ring-shaped outward propagating wave, dependent on resting sea level, and inserted into the paleobathymetry described above. In the bathymetry the crater extended onto land where water was not initially present before impact. We test having a crater purely in water, without the portion of the crater that is formed over land ('Half Crater'), as well as a more complete crater that extended a full 360° onto land, ('Full Crater'), and compare energies, as discussed further below. The fiducial model employs the 'Half Crater' bathymetry. More information on the blending of the hydrocode results into the paleobathymetry is given in SI.

To test sensitivity to the horizontal grid spacing of the shallow-water model, we run a shallow-water simulation at 1/5° grid spacing and compare snapshots of two-dimensional sea surface height perturbation fields (SI Fig. 3) and energies (SI Fig. 4) between this run and the nominal 1/10° run. To test for the sensitivity of the transfer point ("hand-off") between the hydrocode and ocean model, we run a hydrocode simulation, with a larger mesh, out to 850 seconds before emplacement of the hydrocode conditions in the MOM6 model. More details can be found in SI.

3.2 Results

Both shallow-water propagation models are run using the same fiducial run initial conditions and bathymetry data. Snapshots of the MOM6 and MOST sea surface amplitudes are compared at the same times to ensure consistency of the results. The models display similar tsunami propagation patterns (Fig. 3). The main dissimilarities in the model behaviors are in the later-stage wave dynamics. The differences reflect different numerical implementation of the shallow-water wave equations used in the two models. MOST is using the Godonov-type method (a Riemann solver) with a directional splitting, which emphasizes wave characteristics, and a discretization of non-linear terms in Lagrangian form. MOM6 employs vector invariant equations using an energy conserving discretization, with an emphasis on a well-behaved spectra in a turbulent cascade (not resolved or relevant to this problem). In addition, the bottom dissipation is parameterized differently in the two models. MOM6 displays more short-wavelength features after the initial, highest amplitude wave passing. Additional differences arise from different treatments of the north and south boundaries by MOM6 (reflecting boundaries) and MOST (absorbing boundaries without reflection). These model differences do not affect the leading order wave dynamics. The impact tsunami spread outside the Gulf into the Atlantic after about one hour from impact (Fig. 3a); after 4 hours, through the Central American seaway, the waves enter into the Pacific (Fig. 3b); after 24 hours of propagation, the waves cross most of the Pacific from the east and Atlantic from the west and entered the Indian Ocean from both sides (Fig. 3c). The tsunami front propagates in excess of 200 m/s in deep water, in accordance with the shallow-water celerity. By 48 hours post-handoff, e.g., 48 hours after the handoff from the hydrocode to the shallow-water model, significant tsunami amplitudes have reached most of the world coastlines creating a complex amplitude pattern due to wave reflection and refraction (Fig. 3d). Due to wave shoaling the open ocean amplitudes can multiply many-fold near coastlines. The open-ocean amplitudes in most of the Gulf of Mexico are computed to be over 100 m. Along many North Atlantic coastal regions and some South America Pacific coastal regions the models show over 10 m offshore amplitudes. The simulations predict that most of the world ocean experiences maximum offshore amplitudes above 1 m, with the exception of some areas in the Indian Ocean and Mediterranean. Any historically documented tsunamis pale in comparison with such global impact. Depending on the geometries of the coast and the advancing waves, most coastal regions would be inundated and eroded to some extent. The simulations used here do not include wave run-up onto land, as the model resolution of 1/10º is too low to resolve details of the inundation dynamics.

The maximum wave amplitudes and flow velocities (current speeds) at each model grid cell, over the two-day time period of the MOST simulation, are respectively shown in Figs. 4a and 4b. The largest waves and current speeds are in the Gulf of Mexico, North Atlantic, and South Pacific. Near the point of impact, the flow velocity exceeds 100 m/s. In other basins, flow velocities are up to a factor of 100 times smaller in the middle of the ocean than they are near the impact origin and along the coasts. Flow velocities above 20 cm/s are expected to cause erosion of fine-grained pelagic sediments (Lonsdale and Southard, 1974; McCave, 1984). Velocities higher than 20 cm/s are predicted in offshore areas of the North Atlantic and the equatorial region of the South Atlantic, in the Central American seaway and in most of the southern and southwestern Pacific, more than 12,000 km from the impact area. Most coastal areas of the world experienced above-20-cm/s velocities. As discussed in SI, tsunami propagation and flow velocities of simulations with slightly different input configurations (varying model resolution, friction coefficients, hand-off times between hydrocode and shallow-water models, crater size, etc.) are also tested for sensitivity. The energy of the tsunami is not greatly changed in any of these sensitivity tests except for the case in which the rim wave is removed.

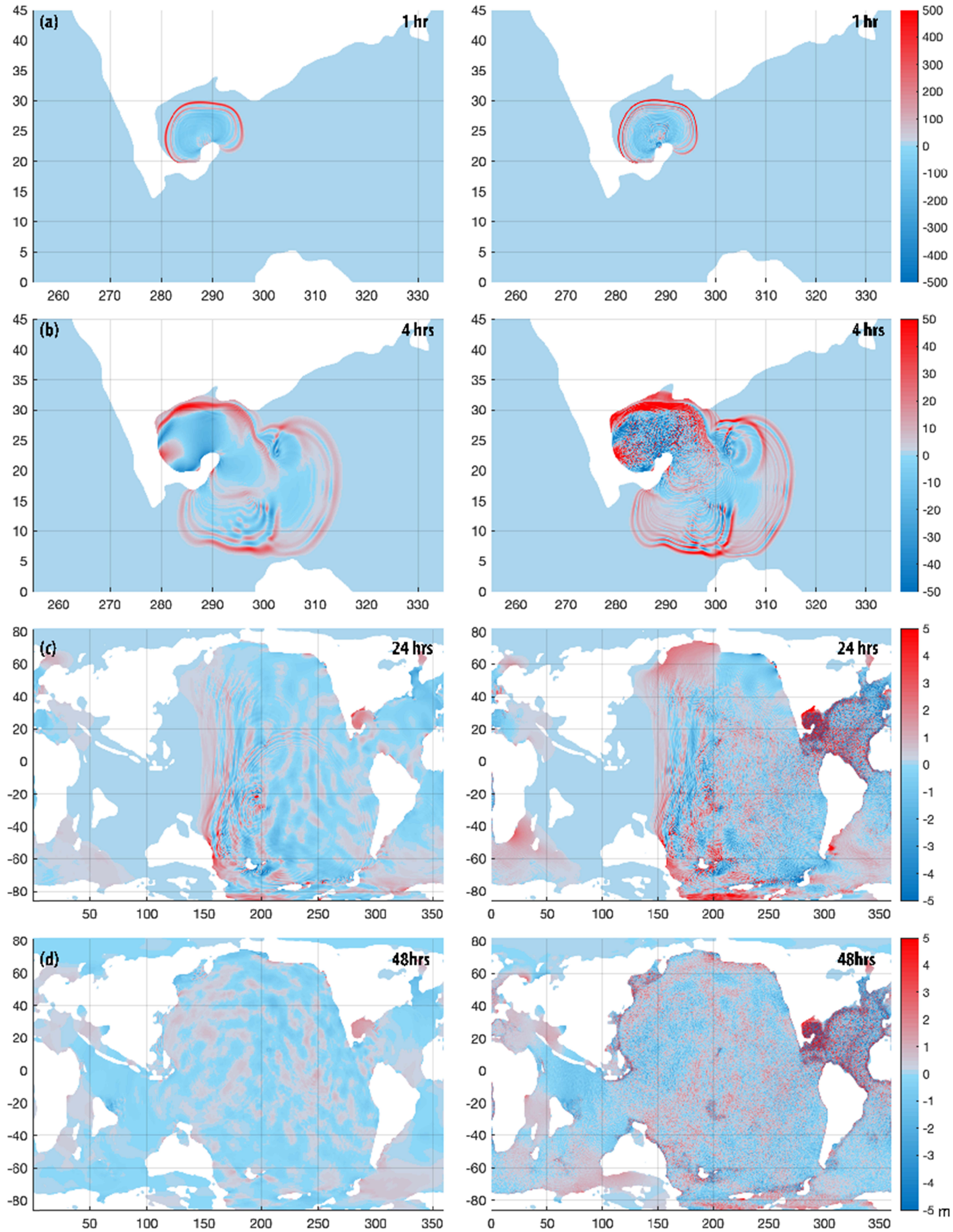

Figure 3. Comparison of two tsunami propagation models: MOST model – left column, MOM6 – right column. Sea surface height perturbation in meters shown at 1 hour (a) and 4 hours (b) after impact around Gulf of Mexico, 24 hours (c) and 48 hours (d) post-handoff globally. Animations for both models are provided in SI Videos 3 and 4.

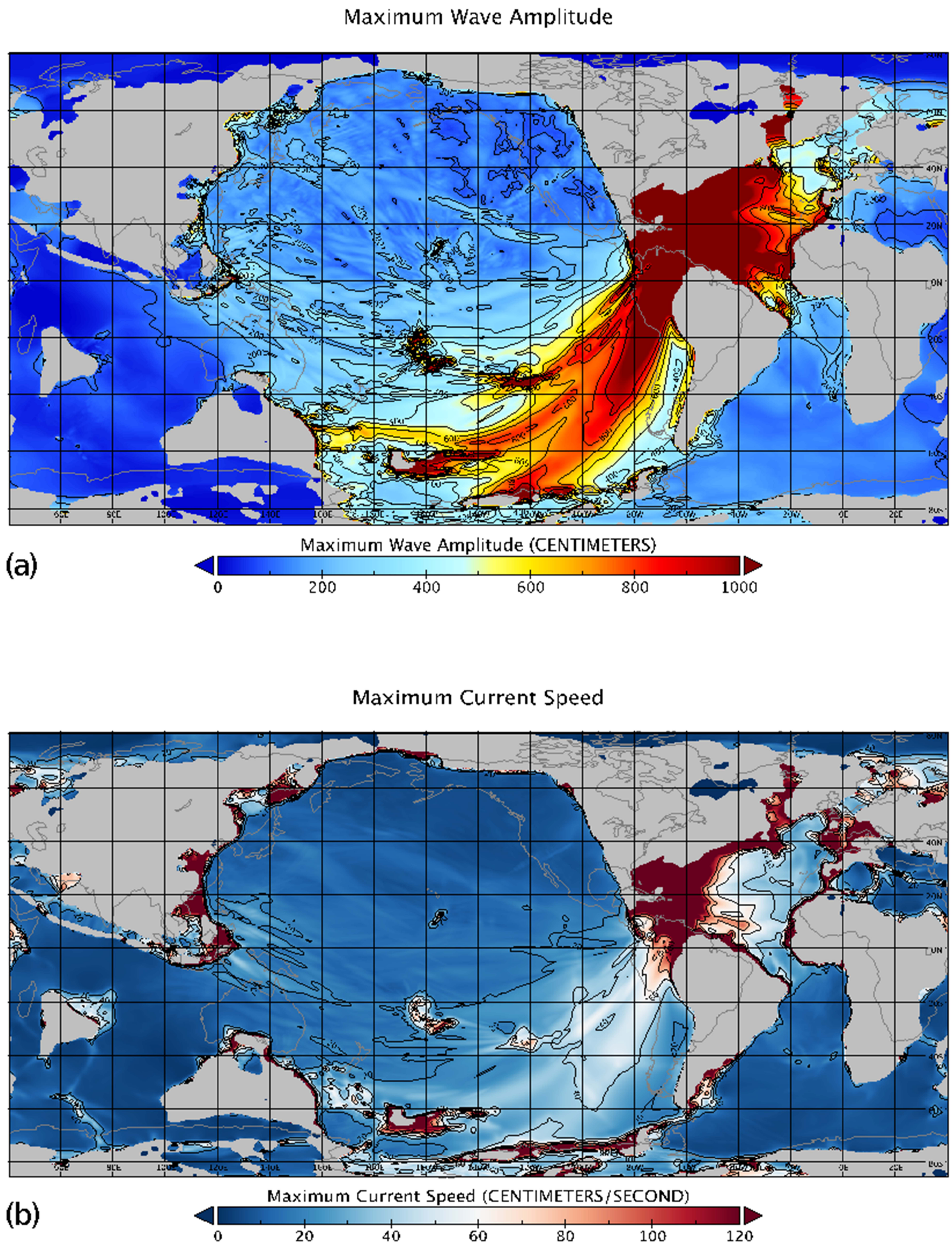

Figure 4. Maximum tsunami sea surface perturbation heights (a) and maximum flow velocity (b) at each grid cell. Contours are shown for every meter of amplitude (saturated at 1000 cm) and every 20 cm/s of speed. Contours of modern continents are shown for reference as gray lines. The results of the MOST model are shown here, because MOST saves values more frequently than MOM6.

4. Geologic Verification of the Models

4.1 Methods

Identifying the K-Pg boundary in marine sections requires some form of stratigraphic information. This is usually provided by biostratigraphic or paleomagnetic investigations. Marine sections located above present-day sea level and exposed on land usually allow a broad view of boundaries in outcrop and extensive stratigraphic data can often be collected from the section. Based on these studies and the overall preservation and exposure of the interval, one section has been named the "type section". The stratotype section for the K-Pg boundary is at El Kef, Tunisia (XXVIIIth International Geological Congress, 1989). The boundary itself has been linked to the anomalous abundance of Iridium that was derived from the impacting body.

Close to the impact site reworked sedimentary deposits are mixed with ejecta from the impact. At intermediate distances the airborne ejecta may have arrived before the tsunami; thus, airborne ejecta with higher Iridium concentrations may lie below rip up clasts and redeposited older sediments. In distant regions, high concentrations of Iridium used to define the K-Pg boundary (Kiessling & Claeys, 2002) are thought to have arrived by settling from the stratosphere over a period up to several years (Claeys et al., 2002; Toon et al, 1982). This is compared to the modeled tsunami reaching a global extent in just two days. To verify the strength and pathway of the modeled impact tsunami we pay particular attention to these more distal regions (Schulte et al. 2010). In these regions the effects of the tsunami should be found in the interval immediately below the K-Pg boundary itself in both marine sections on land (supplementary table ST-1) and in scientific ocean drilling cores (supplementary table ST-2). We take any sign of missing biostratigraphic or paleomagnetic intervals or depositional disturbance immediately below this level (e.g., erosional truncations of bedding or bioturbation features, sediment deformation, allochthonous clumps or clasts) as evidence of current activity or disturbance associated with the impact tsunami.

A few of the studied boundary sections have paleomagnetic stratigraphy. The K-Pg boundary has been found to be within the upper half of subchron C29r in Gubbio, Italy (Lowrie and Alvarez, 1977) and Agost, Spain (Canudo et al., 1991). The estimated duration of the Cretaceous part of subchron C29r is 300 kyr (Husson et al. 2011). Biostratigrapy often provides an important indication of missing section in deeper water, pelagic sections. The *Abathomphalusmayaroensis* Zone defines the uppermost Cretaceous foraminiferal zone in many of the older studies of the K-Pg boundary; however, Keller (1988) found that

A. mayaroensis disappeared below the K-Pg boundary in the type section at El Kef. To fill this gap, Pardo et al. (1996) defined a total range biozone (*Plummerita hantkeninoides*) that marks the top of the Maastrichtian and lies within the lower half of subchron C29r. The uppermost Cretaceous nannofossil zone is defined by the range of *Micula prinsii* (Sissingh, 1977). This Zone occupies most of the lower half of subchron C29r. Other fossil assemblages have been used to evaluate the ages within the Late Cretaceous, but they have not been well documented in more than one or two complete K-Pg boundary sections. Carbon and oxygen isotope stratigraphies have been generated for several of the K-Pg boundary sections (Supplementary Tables ST-1, ST-2). The records of the carbon isotopes show an abrupt break at the K-Pg boundary, with the isotopes becoming sharply negative (a drop of 2‰ at El Kef; Keller and Lindinger, 1989). However, the oxygen isotopes signal is more variable and may depend on what microfossils are being measured (c.f. El Kef, in Keller and Lindinger, 1989; MacLeod et al., 2018, and other sections in Caravaca, in Canudo et al., 1991; and in Zumaia, in Margolis et al., 1987).

The advent of orbital tuning of geologic records has greatly advanced our ability to develop estimates of ages with comparable precision well back into the Cretaceous (e.g., Batenburg et al, 2012; Dinarés-Turrel et al., 2014; Husson et al., 2011 and references therein).These studies use calculated variations in the earth's orbit as a template for matching variations in stable isotopes, color, iron content, or bed thickness; however, beyond 60 Ma only the 405 kyr eccentricity cycle is known with sufficient accuracy to be used in tuning the time scale (Laskar et al., 2011; Westerhold et al., 2012). From these tuning efforts we know that the K-Pg boundary lies at the top of the 405 kyr orbital cycle of eccentricity designated as Ma405 1 (Batenburg et al., 2012). Any effort at tuning must take place within a stratigraphic framework defined by other tools, normally a paleomagnetic stratigraphy, which in turn usually relies on a biostratigraphic framework.

For the drill sites reported in this study, we list those sites (Supplementary Table ST-2) in which the K-Pg boundary interval is recovered and is fossiliferous, with stratigraphies that define the location of that boundary. Based on stratigraphic evaluations for both drilled cores and outcrop sections, we class the K-Pg boundary sections as: 1) complete, 2) apparently complete, 3) having a detectable depositional disturbance, hiatus, or disconformity, or 4) having a long erosional hiatus or non-depositional surface (Fig. 5). If such long missing sections range from the Cretaceous well up into the Paleocene or even younger sections, we cannot claim that they are attributable to the impact tsunami (category 4, above), and we discount them from our analysis. If, however, the lower part of the Paleocene is present, while a part of the Upper Cretaceous is missing, we classify this as possibly caused by the impact tsunami (category 3, above).

4.2 Results

The devastating effects of the asteroid impact in the Caribbean and Gulf of Mexico included earthquakes, slope failures, and debris flows, all of which could have contributed to tsunami formation, (e.g., Alegret and Thomas, 2005; Alvarez et al., 1992, 1995; Bourgeois et al., 1988; Bralower et al., 1998; Campbell et al., 2008; Denne et al., 2013, Keller et al., 1997, 2007; Kinsland et al., 2021; Maurrasse et al., 1991; Montanari et al., 1994; Schulte et al., 2006, 2008; Smit et al., 1996; Sanford et al., 2016; Stinnesbeck et al., 1997). These ancillary effects are not accounted for in the impact tsunami models, but nevertheless disrupted the K-Pg boundary. The modeled impact tsunami took principal radiation pathways directed to the east and northeast into the North Atlantic and to the southwest, through the Central American passage and into the southwestern Pacific (Fig. 4). At flow speeds greater than 20 cm/sec (Fig. 4b) the passing tsunami could have eroded fine-grained marine sediment even on the deep seafloor (Lonsdale and Southard, 1974; McCave, 1984).

The Tethys region, the South Atlantic, the North Pacific, and the Indian Ocean basins were largely shielded from the stronger effects of the tsunami (Fig. 4). This is consistent with the location of the several complete sections described from the marine outcrops around the Mediterranean, including the type section at El Kef (Fig. 5). It is also consistent with the frequent recovery of complete sections at scientific ocean drilling sites in the South Atlantic Ocean and on Seymour Island in the Antarctic Peninsula, the several complete sections of the K-Pg boundary recovered in the North Pacific Ocean and on the island of Hokkaido, and the complete K-Pg boundary intervals drilled on bathymetric highs in the eastern Indian Ocean.

Looking at K-Pg boundary intervals that lay in the modeled pathway of the tsunami, the results of the comparison are also largely consistent. The drilled sections in New Jersey show gaps, rip up clasts, or tempestites in the K-Pg boundary interval. Sections studied in western Europe (Germany, Denmark, France, Bulgaria, Austria; Supplementary Table ST-1) generally show biostratigraphic gaps, erosional truncations, or slumps and gravity flows in the uppermost part of the Maastrichtian section. In the North Atlantic Ocean only three sites in two areas contain what appear to be complete K-Pg boundary intervals (Fig. 5). Site U1403 is the deepest site drilled on the J-Anomaly Ridge off Newfoundland. The Upper Cretaceous section is relatively thick here, lying between two southeast trending basement highs (Expedition 342 Scientists, 2012) and may represent a depocenter for sediment eroded from the nearby locations. Sites 1259 and 1260 are located on the slope of the Demerara Rise off Suriname, South

America. During the Late Cretaceous their location was within a few degrees north of the equator and may have been partially shielded from the main force of the tsunami (MacLeod et al., 2007). However, farther south on the coast near Recife, Brazil, at Pernambuco, a neritic section contains a graded sandy bed, including ejecta from the asteroid impact, and is overlain by an iridium anomaly (Albertaõ and Martins, 1996).

Almost all the drill sites in the South Pacific basin appear to have a missing uppermost Maastrichtian section. This is true even on the southern part of the Ongtong-Java Plateau, which lies near the northern edge of higher velocities associated with the impact tsunami's modeled pathway, while two sites on the northern side of the Plateau (Sites 803 and 807) have the only complete K-Pg sections recovered in the South Pacific basin of 65 Ma (Figs. 4b, 5).

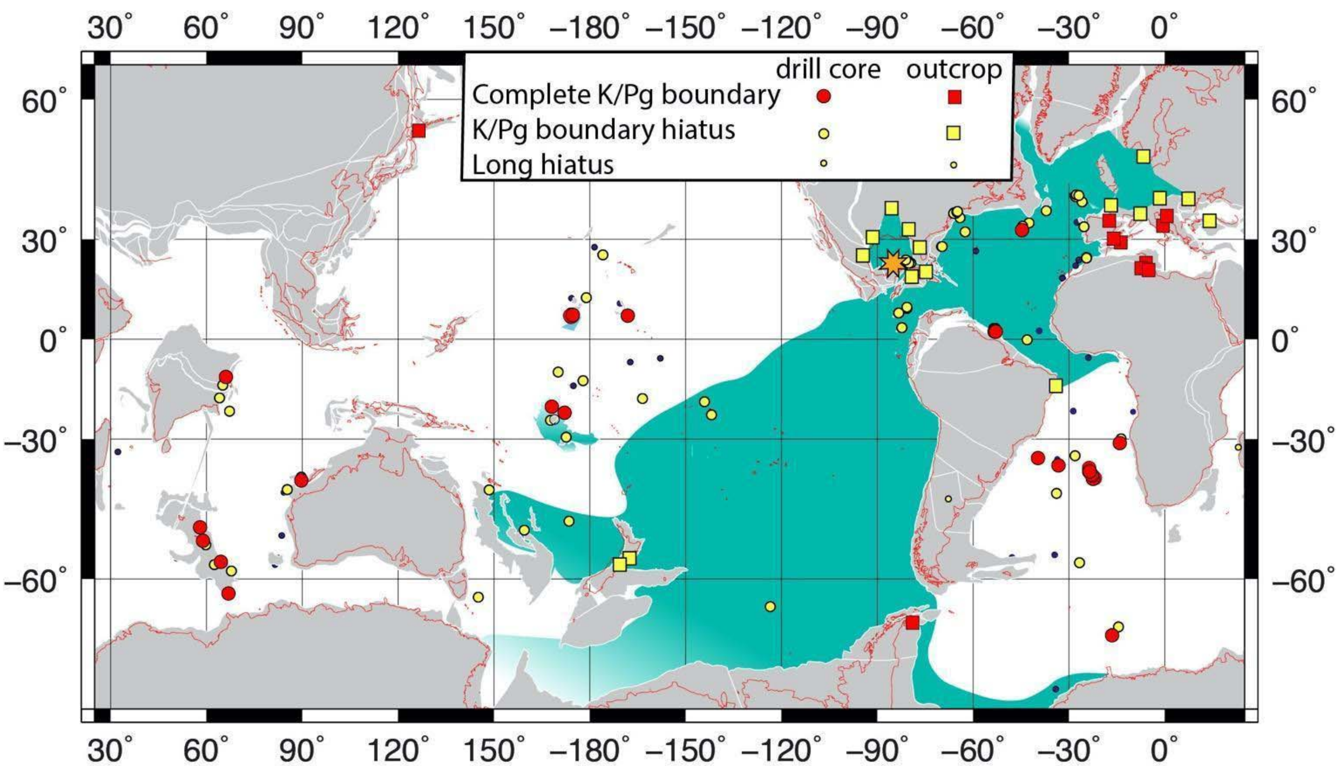

Figure 5. Plate reconstruction and site locations at 65 Ma from ODSN website (http://www.odsn.de/odsn/services/paleomap/paleomap.html) using the magnetic reference frame. Continental blocks in gray with modern continental outlines in red. Green shaded ocean areas depict approximate regions where the models of the K-Pg impact tsunami showed flow velocities in excess 20 cm/sec (see Fig. 4b). Most coastal regions were indicated by the models to have experienced such high velocities, but are not shown here. Drill site locations indicated by circles; K-Pg land outcrop sites indicated by squares (see legend). Small filled circles indicate sites with hiatuses of a million years or more duration that span the K-Pg boundary and range well into the Paleogene.

Of particular interest are the outcrops of the K-Pg boundary interval on the southeast corner of North Island and northeast corner of South Island, New Zealand. Here the olistostromal deposits at the top of the Upper Cretaceous Whangi Formation were originally explained as the result of local tectonic activity (Laird et al., 2003) or mass flow deposit (Hines et al., 2013); but considering the stratigraphic position of this deposit and its location directly in line with the modeled pathway of the impact tsunami, we feel the olistostrome is recording the effects of the impact tsunami (Figs. 4, 5, 6). Hollis (2003) reviewed 16 marine sections in New Zealand that ranged in paleo water depth from inner shelf to upper bathyal and found that at least 14 of them probably had a missing or disturbed K-Pg boundary interval. However, detailed biostratigraphic control of the uppermost Maastrichtian is lacking for the remaining two sections, which raises the possibility that these sections may also be incomplete. Paleomagnetic control on the sections has not been obtained due to pervasive demagnetization (Kodama et al., 2007).

The tsunami models indicate that many coastal regions around the globe may have been affected by the impact tsunami; however, without a detailed knowledge of the bathymetry and coastal geometry at the end of the Cretaceous, and without a higher resolution model in these areas, we cannot evaluate how accurate the models might be in such shoreline areas. Our study shows that some distant near-shore areas were strongly affected (e.g., New Jersey, New Zealand, Pernambuco), while others were not (e.g., Seymour Island, Hokkaido). Still, it is probably significant that the models show only minor coastal effects in the shielded Tethys basin (Fig. 5, 6) where all the neritic sections appear to be complete (Supplementary Table ST-1).

In a similar manner, all the large, relatively shallow oceanic plateaus and rises show up in the higher velocity regions of the models (Fig. 4b); however, as in the coastal regions, the resolution of the models and that of the paleo bathymetry do not allow detailed comparison of the model results with the completeness of the recovered sections. We feel it is significant that only those prominent bathymetric highs that lie outside the main pathway of the impact tsunami show a preponderance of complete K-Pg sections (Figs 4b, 5).

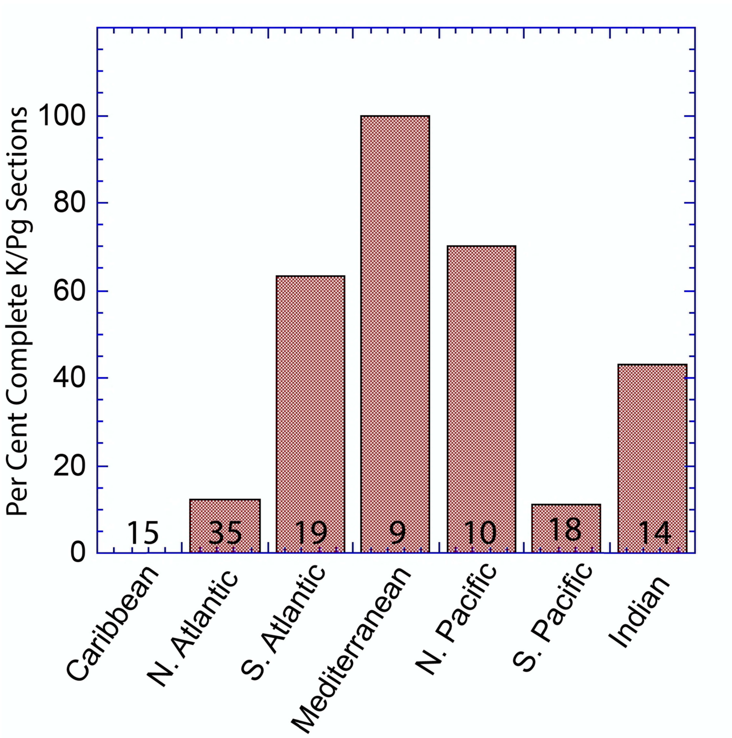

Figure 6. The percent of apparently complete marine sections containing the K-Pg boundary interval listed by ocean basin, including both marine sections found on the surrounding land and in scientific ocean drilling cores. Data do not include sites with long hiatuses (see text). The number of sections studied is shown at the base of each column (see Supplementary Tables ST-1 and ST-2). No complete sections were found in the Caribbean (including the Gulf of Mexico). The South Atlantic and South Pacific categories include sites studied in the Southern Ocean sector of these basins.

A summary of the studied marine sections on land and in drill cores is shown in Figure 6. As noted above, all marine sections on land around the Mediterranean lie outside the modeled >20 cm/sec flow velocity contour (Fig. 4b, 5) and are believed to have complete K-Pg boundary records. Also noted above, the Caribbean-Gulf of Mexico region lies within the area of very high flow velocities and have no complete, undisturbed sections. Similarly, the North Atlantic Basin is an area of high flow velocities and has only four sites (11% of sites studied) that are apparently complete (ST-1, ST-2). The South Pacific region with flow velocities > 20 cm/sec Figs. 4b, 5) have two sites (11% of sites studied) that appear to be complete.

At least 65% of the studied sections in regions where modeled flow velocities are <20 cm/sec have complete sections. In regions with flow velocities >20 cm/sec, 91% of the studied sections have incomplete K-Pg boundary sections. The most telling confirmation of the global significance of the impact tsunami is the highly disturbed and incomplete sections on the eastern shores of North and South Islands of New Zealand. These sites lie directly in the path of the tsunami propagation, more than 12,000 km distant from the impact location (Figs. 4, 5).

5 Discussion

5.1 Tsunami Mechanisms

Earlier theoretical and regional simulations (e.g., Ward, 2012; Matsui et al., 2002; Wünnemann and Weiss, 2015) differ on whether the rim wave or collapse wave dominates with respect to energy. The rim wave refers to the water displaced from the impact that is pushed away from the origin (Wünnemann and Weiss, 2015). The collapse wave is the secondary process arising from the cavity collapse in the crater and water rushing into the crater (Wünnemann and Weiss, 2015). To test the relative contributions of the collapse and rim waves to the total tsunami energy, we ran a simulation ('Crater Only') with no rim wave or velocity, such that the tsunami is solely due to the collapse wave filling in the crater. Our results agree with the conclusion of Wünnemann and Weiss (2015), that the rim wave is the source of most of the energy for this impact tsunami. Four hours after impact, the 'Crater Only' case is about 13 times less energetic than the 'Full Crater, With Rim Wave' case. The MOM and MOST model simulations of the Full Crater scenario showed similar energy numbers four hours post-handoff (3.90×10^{19} and 3.84×10^{19} J correspondingly), such that the model energy estimates appear to be robust and independent of the exact model used.

The efficiency of tsunamis can be quantified by the ratio between tsunami energy and the source energy. The efficiency of tsunami generation by the Chicxulub impact is similar to that of large earthquakes. The energy ratio for earthquake-generating tsunamis averages around 0.1% (with large variations from 0.02% to 0.8%, Tang et al., 2012), while we predict that the Chicxulub tsunami has an efficiency of 0.19% (SI Table 4). SI Figure 4 shows that the impact tsunami energy dissipates relatively quickly, relative to seismogenic tsunamis, consistent with the "Van Dorn effect" (Van Dorn et al., 1968) of faster wave energy attenuation due to large non-linearities near the source of explosion-generated tsunamis. Near-field tectonic activity, triggered by passage of strong stress wave produced by the impact, was not included in our simulations. It is likely that any earthquake generated slides and collapses would be minor relative to the primary rim wave.

5.2 Hiatus Distribution

The better preserved, thicker, carbonate-rich sections in the oceans are commonly found on bathymetric highs such as continental terraces, oceanic plateaus, rises, aseismic ridges, and seamounts. Drill sites in which the K-Pg boundary is clearly identified are usually found in such locations. These locations do have their own problems, however. Such regions of bathymetric prominence also give rise to enhanced turbulence in the waters surrounding them (Cacchione & Drake, 1986; Cacchione et al., 2002; Rudnick et al., 2003; Wunsch & Ferrari, 2004); thus, they enhance the erosional power of tsunamis and tidal waves that pass over them. The preserved sedimentary sections atop bathymetric highs usually show clear evidence of erosion and the sculpting of pelagic deposits that sit upon them. The drilling strategy often employed by scientific ocean drilling expeditions takes advantage of the stratigraphic character of these deposits to sample relatively older intervals where overburden has been removed or was never deposited, the intention being to minimize the effects of diagenetic alteration on these older sediments. At other sites, full advantage was taken of the thicker, more complete sections to study the detailed paleoceanographic history. This duality of purpose means that many sites drilled on bathymetric highs contain significant gaps in the stratigraphic record, while on some highs there are close-by sites that have recovered complete sections. In regions with modeled flow velocities < 20 cm/sec, several sites locate the K-Pg boundary between recovered cores (ST-2); thus, the amount of missing section (if any) and the exact nature of the boundary is uncertain.

In basins where almost all sites show incomplete uppermost Maastrichtian sections there are still a few deep-sea sections that appear to be complete (e.g., Sites 1259, 1260, U1403 in the North Atlantic). These may represent local bathymetric shielding from erosion or local depocenters that receive sediment which has been eroded from nearby areas. The coincidence of regions having few if any complete K-Pg boundary sections and the pathway of relatively strong tsunami flow, combined with the more common occurrence of complete K-Pg boundary sections in regions that did not have strong tsunami flow, support the results of the tsunami models. The lack of complete K-Pg boundary sections in the southern South Pacific and on the eastern shores of New Zealand strongly suggest that this tsunami was of global significance, reaching at least 12,000 km across the deep ocean. It also suggests that except for some shallow coastal regions, areas such as the Tethyan region, the North Pacific, the South Atlantic and much of the Indian Ocean basin were largely geographically shielded from the effects of the tsunami

5.3 Comparison with Large Historical Tsunamis

To provide perspective on the size of the impact tsunami, we compare our impact tsunami model estimates with some representative large historical tsunamis. The 2004 Indian Ocean tsunami (Smith et al., 2005) is possibly the largest modern-era tsunami; it killed over 230,000 people around the Indian Ocean and was recorded around the globe (Titov et al., 2005). The 2011 Tohoku tsunami was generated by a similarly strong earthquake and has become the costliest natural disaster of all time. Offshore amplitudes of the

2004 Indian Ocean tsunami 2 hours after generation were measured to be about 0.6 m, and 2 meter waves were measured about 500 km away from the epicenter of the 2011 Tohoku tsunami, at a seafloor depth of 5700 m. These deep-ocean amplitudes led to runup at coastlines of up to 40 m (Sumatra Island) and 50 m (Honshu Island). The 1883 Krakatau event generated another catastrophic tsunami with explosive-type initial conditions, potentially similar to the impact generation. The Krakatau wave devastated local coastlines, killing over 30,000 (second most deadly record after the Indian Ocean tsunami) with waves that ran up to 40 m and traveled distances of up to 5 km inland, but did not generate significant waves outside Sunda Strait. All these tsunamis, among the largest in recorded history, are dwarfed by the wave amplitudes and energy of the simulated Chicxulub tsunami. The Chicxulub tsunami produces offshore amplitudes over 1 m around most of the world oceans (Figure 4a). When tsunamis reach the shallow waters of a coastline or bathymetric high, wave amplitude increases due to shoaling. Comparison of our tsunami simulations with observations and modeling of the strongest recent tsunamis of 2004 and 2011 implies that the coastal amplitudes for the Chicxulub tsunami would flood most coastlines, in a manner that would be catastrophic in modern times. The total energy of our impact tsunami simulations is compared with the energy of these large historical tsunamis in SI Table 4 and SI Figure 4. Energy values are calculated according to standard formulae for shallow-water energy (e.g., Arbic et al., 2004; their equation 14). SI Figure 4 displays the ratios of energy in the impact tsunami simulations to the 2004 Indian Ocean tsunami, as a function of time into the ocean simulation. The energy in the impact tsunami decays faster than the energy in the 2004 Indian Ocean tsunami – another manifestation of the "Van Dorn effect". The initial energy in the impact tsunami was up to 30,000 times larger than the energy of any historically documented tsunamis. Wave energies in the 'Half Crater' simulation are about 5% less than those in the 'Full Crater' simulation. The 'Crater Only' simulation, without the large rim wave, still has much more energy than any other historical tsunamis. For a wide variety of sources, the portion of the source energy that goes into tsunami generation is less than 1%, with large variations from about 0.01% to 0.3% (SI Table 4). An impact- and explosion-type of tsunami generation appears to have similar efficiency in transferring energy into long wave propagation. However, impact- and explosion-generated tsunamis dissipate energy much faster during propagation. Nevertheless, the sheer amount of energy of the impactor is sufficient to generate a giant global tsunami, even if only 0.2% of the impact energy goes into the tsunami.

5.4 Future work

The first global simulation of the Chicxulub impact tsunami demonstrates that it was much larger than any recent earthquake-generated tsunami, and that it was likely large enough to leave a mark on marine sediment records. Many uncertainties remain, and there is much room for improvement in future studies. It is well known that most impacts are oblique with 45° impact angle being most likely (e.g., Robertson et al., 2021). With sufficient computer power, high-resolution, three-dimensional hydrocode simulations of the first ten or so minutes could be performed, thus allowing for varying water depth, non-perpendicular impact angles, and other key uncertainties in the hydrocode simulation. Generally, we would expect a slightly larger rim wave in the downrange direction and a smaller wave up range. It may be instructive to vary initial conditions of the global simulation in a parameterized way to crudely account for impact angle.

The January 15, 2022, Hunga Tonga-Hunga Ha'apai volcano explosion has demonstrated an additional mechanism of tsunami generation from large explosive events – the low frequency air pressure wave, e.g. Lamb wave (Duncombe, 2022). While the exact mechanism of the air pressure Lamb wave is not fully understood, it is clear that significant waves can be generated from such air pressure waves propagating over oceans. The full analysis of such tsunami generation is out of the scope of this paper and is a subject of future research. But based upon observations and initial modeling of the Tonga event, it is clear that the Lamb wave can be a source of significant secondary tsunamis around the world. These waves would reach world coastlines much earlier than the tsunami generated by the crater formation. The energy of the Chicxulub impact is at least 100,000 times larger than the Tonga explosion. The Lamb wave from the Tonga explosion generated tsunami waves of over a meter at some locations around the Pacific and up to half a meter at other oceans. Thus, the Lamb wave from the Chicxulub explosion can be a significant source of tsunamis in the far-field from the impact source, and will be a subject of future work.

Dispersive effects may manifest themselves in the Chicxulub tsunami propagation simulations in two ways: (1) during the long-distance propagation as different wave frequencies separate from a single front; and (2) during the evolution of the initial steep wave front into an undular bore (Glimsdal et al., 2007). Tsunami amplitudes in shallow water wave approximation models may overpredict shorter dispersive waves or underpredict sharp frontal amplitudes experiencing fission and undular bore formation. In both cases the difference may be up to 50% of amplitudes in certain cases (see for example Son et al., 2011, Zhou et al., 2014, 2012). Addressing these effects is a topic for future research.Both of these processes generally lead to the decrease of amplitudes in comparison with the classic shallow-water wave theory estimates. Therefore, the non-linear shallow water approximation provides, in general, a conservative (upper-bound) estimate of potential tsunami amplitudes. The use of Boussinesq-type models may provide a better resolution of the undular bore feature of the turbulent wave front. However, tThese effects involve generation of much shorter (therefore much more dissipative) wavelengths that are usually confined to a relatively small part of the wave near the bore front (see for example Son et al., 2011, Matsuyama et al., 2007), and therefore may have very limited effect on the global wave propagation pattern – the main goal of this study. Also, the results of Glimsdal et al. (2007) show that the Boussinesq model appears to overestimate the dispersive front effects in comparison with the full hydro code, which may be attributed to difference in resolution or to the inherent tendency of Boussinesq models to overestimate dispersion. The detailed modeling of the dispersive front of the leading tsunami with higher spatial resolution dispersive simulations would show more precise dynamics of the tsunami in the near-source area and may change the details of the maximum amplitude distribution near the source. Therefore, such studies with higher resolution dispersive models would be a natural extension of this work, especially for more precise estimates of tsunami impact within the Gulf of Mexico. However, we don't expect these details to significantly change our far-field estimates of the tsunami amplitudes and tsunami energy directionality (Zhou et al., 2012, 2014).

In the case of our modeling, we expect the dispersive effects would be, at least partially, accounted for, since one of the models (MOST) includes the physical process of frequency dispersion approximated by numerical dispersion (Burwell et al., 2007). MOST has been benchmarked against laboratory tests with highly dispersive and highly non-linear waves for wave breaking dynamics (Titov and Synolakis, 1995) and compared with dispersive models during the long-distance tsunami propagation (Zhou et al., 2012). These comparisons showed that MOST provides results closely resembling the dispersive models estimates. The consistency of MOST and MOM6 results provides confidence in the robustness of our results. However, dispersive effects as well as uncertainties such as in the details and size of the impactor, and in the paleo-bathymetry estimates should be investigated more fully in future work.

Acknowledgments, Samples, and Data

Supplementary Information is linked to the online version of the paper.

Acknowledgments: We thank Gareth Collins, Finn Løvholt, Clemens Rumpf, and two anonymous reviewers for comments and suggestions that led to significant improvements in the manuscript. B.K.A. thanks Sarah Stamps for useful conversations. M.M.R. and B.K.A. thank Mark Champe, Charles Antonelli, and Michael Messina for help with setting up MOM6 on University of Michigan computers. M.M.R., B.K.A., and J.K.A. acknowledge funding support from US National Science

Foundation grants OCE-0968783 and OCE-1351837, a Research Experience for Undergraduates (REU) supplement for MMR to OCE-1351837, and the University of Michigan Associate Professor Support Fund supported by the Margaret and Herman Sokol Faculty Awards. We gratefully acknowledge the developers of iSALE-2D, including Gareth Collins, Kai Wünnemann, Dirk Elbeshausen, Tom Davison, Boris Ivanov and Jay Melosh. Some plots in this work were created with the pySALEPlot tool written by Tom Davison. The MOM6 simulations in this paper were carried out on the Flux supercomputer provided by the University of Michigan Advanced Research Computing Technical Services. Much of B.K.A.'s contributions to this paper took place while he was on sabbatical in France. B.K.A. thanks many French colleagues, especially Thierry Penduff, Rosemary Morrow, Nadia Ayoub, and Florent Lyard, for their help in procuring this sabbatical year. He Wang's contributions from GFDL are supported by NOAA's Science Collaboration Program and administered by UCAR's CPAESS under awards NA16NWS4620043 and NA18NWS4620043B. This is contribution number 5300 of NOAA-PMEL. Results, bathymetry, and initial conditions of our work can be found at https://doi.org/10.7910/DVN/GWOFIO.

Author Contributions: M.M.R. converted the hydrocode results into the initial conditions for the MOM6 tsunami simulations, ran the MOM6 simulations, and wrote the paper. B.K.A. oversaw the project. B.C.J. ran the iSALE hydrocode simulations and greatly contributed to the design of the final simulations. T.C.M. conceived the project in a conversation with B.K.A. Together with C.J.H. he provided geologic information on the studied K-Pg sections. V.T. ran the MOST simulations and guided comparisons of MOST and MOM6 results. A.J.A., J.K.A., and H.W. helped M.M.R. set up and run the MOM6 model on University of Michigan computers. J.K.A. also helped M.M.R. to construct initial conditions. J.R. initiated discussions that greatly improved our initial conditions and eventually led to the use of iSALE. C.R.S. provided the bathymetry for the K/Pg Boundary. All authors contributed to improving the manuscript.

The authors declare no conflict of interest.

References

Adcroft, A. (2013). Representation of topography by porous barriers and objective interpolation of topographic data. *Ocean Modelling,* 67, 13-27, https://doi.org/10.1016/j.ocemod.2013.03.002.

Adcroft, A. (2017). NOAA - GFDL MOM6 Examples, *Github*. Available from: https://github.com/NOAA-GFDL/MOM6-examples/wiki

Albertao, G.A., & Martins Jr., P.P. (1996). A possible tsunami deposit at the Cretaceous-Tertiary boundary in Pernambuco, northeastern Brazil. Sedimentary Geology, 104, 189-201.

Alegret, L. & Thomas, E., (2005). Cretaceous/Paleogene boundary bathyal paleo-environment in the central North PacificDSDP Site 465), the Northwestern Atlantic (ODP Site 1049), the Gulf of Mexico and the Tethys: The benthic foraminiferal record. *Earth and Planetary Science Letters*, 224, 53-82

Alvarez, W., Smit, J., Lowrie, W., Asaro, F., Margolis, S.V., Claeys, P., Kastner, M., & Hildebrand, A.R. (1992). Proximal impact deposits at the Cretaceous-Tertiary boundary in the Gulf of Mexico: A restudy of DSDP Leg 77 Sites 536 and 540. *Geology*, 20, 697–700.

Alvarez, W., Claeys, P., & Kieffer, S.W. (1995). Emplacement of Cretaceous-Tertiary boundary shocked quartz from Chicxulub Crater. *Science,* 269, 930–935.

Anderson, J.LB., Schultz, P.H., & Heineck, J.T. (2003). Asymmetry of ejecta flow during oblique impacts using three-dimensional particle image velocimetry. *Journal of Geophysical Research: Planets,* 108, 5094, https://doi.org/10.1029/2003JE002075.

Arbic, B.K., Garner, S.T., Hallberg, R.W., & Simmons, H.L. (2004). The accuracy of surface elevations in forward global barotropic and baroclinic tide models. *Deep-Sea Research II,* 51, 3069-3101, https://doi.org/10.1016/j.dsr2.2004.09.014.

Bardeen, C.G., Garcia, R.R., Toon, O.B., & Conley, A.J. (2017). On transient climate change at the Cretaceous-Paleogene boundary due to atmospheric soot injections. *Proceedings of the National Academy of Sciences of the United States of America*, *114*(36), E7415–E7424. https://doi.org/10.1073/pnas.1708980114.

Bahlburg, H., Weiss, R., & Wünnemann, K. (2010). Low energy deposition in the Chicxulub crater during the impact to post-impact transition. *Earth and Planetary Science Letters*, 295, 170–176, https://doi.org/10.1016/j.epsl.2010.03.037.

Batenburg, S.J., Sprovieri, M., Gale, A.S., Hilgen, F.J., , Hüsing, S., Laskar, J., Liebrand, D, Lirer, F., Orue-Etxebarria, X., Pelosi, N., & Smit, J. (2012). Cyclostratigraphy and astronomical tuning of theLate Maastrichtian at Zumaia (Basque country), Northern Spain. *Earth and Planetary Science Letters*, 359-360,264-278, https://doi.org/10.1016/j.epsl.2012.09.054

Bell, C., Morgan, J.V., Hampson, G.J., & Trudgill, B. (2004). Stratigraphic and sedimentological observations from seismic data across the Chicxulub impact basin. *Meteoritics & Planetary Science*, *39*(7), 1089–1098. https://doi.org/10.1111/j.1945-5100.2004.tb01130.x.

Bourgeois, J., Hansen, T.A., Wiberg, P.L. & Kauffman, E.G. (1988). A tsunami deposit at the Cretaceous-Tertiary boundary in Texas. *Science*, 241, 567–570.

Bralower, T.J., & Paull, C.K. (1998) The Cretaceous-Tertiary boundary cocktail: Chicxulub impact triggers margin collapse and extensive sediment gravity flow, Geology, 26(4), 331-334.

Brugger, J., Feulner, G., & Petri, S. (2017). Baby, it's cold outside: Climate model simulations of the effects of the asteroid impact at the end of the Cretaceous. *Geophysical Research Letters*, *44*(1), 419–427, https://doi.org/10.1002/2016GL072241

Burwell, D., Tolkova, E., & Chawla, A. (2007). Diffusion and dispersion characterization of a numerical tsunami model. *Ocean Modelling*, 19, 10–30, https://doi.org/10.1016/j.ocemod.2007.05.003

Busby, C.J., Yip, G., Blikra, L., & Renne, P. (2002). Coastal landsliding and catastrophic sedimentation triggered by Cretaceous-Tertiary bolide impact: A Pacific margin example? *Geology*, *30*(8), 687–690, https://doi.org/10.1130/0091-7613(2002)030<0687:CLACST>2.0.CO;2

Cacchione, D.A. & Drake, D. E. (1986), Nepheloid Layers and Internal Waves Over Continental Shelves and Slopes, Geo-Marine Letters, 6,147-152.

Cacchione, D. A., Pratson, L. F. & Ogston, A. S. (2002), The shaping of continental slopes by internal tides, S*cience*, 29, 724-727

Campbell, C.E., Oboh-Ikuenobe, F.E., Eifert, E.I. (2008). Mega tsunami deposit in Cretaceous-Paleogene boundary interval of southeastern Missouri. *Geological Society of America Special Paper* 437, 189-198.

Canudo, J.I., Keller, G., & Molina, E. (1991). Cretaceous/Tertiary boundary extinction pattern and faunal turnover at Agost and Caravaca, S.E. Spain. *Marine Micropaleontology*, 17, 319-341. https://doi.org/10.1016/0377-8398(91)90019-3

Claeys, P., Kiessling, W., & Alvarez, W. (2002). Distribution of the ejecta at the Cretaceous- 607Tertiary boundary, In C. Koeberl & K. G. MacLeod, (Eds.) Catastrophic events and mass 608 extinction: impacts and beyond. *Geological Society of America Special Paper 356*, 55–69. 609

Collins, G.C., Melosh, H.J., & Ivanov, B.A. (2004). Modeling damage and deformation in numerical impact simulations. *Meteoritics and Planetary Science*, *39*(2), 217–231, https://doi.org/10.1111/j.1945-5100.2004.tb00337.x

Collins, G.S., Patel, N., Davison, T.M., Rae, A.S. P., Morgan, J.V., Gulick, S.P S., et al. (2020) A steeply-inclined trajectory for the Chicxulub impact. *Nature Communications* 11, 1480. https://doi.org/10.1038/s41467-020-15269-x.

Collins, G.S., Morgan, J., Barton, P., Christeson, G.L., Gulick, S., Urrutia, J., Warner, M., & Wünnemann, K. (2008). Dynamic modeling suggests terrace zone asymmetry in the Chicxulub crater is caused by target heterogeneity. *Earth and Planetary Science Letters*. https://doi.org/10.1016/j.epsl.2008.03.032

Denne, R.A. , Scott, E.D., Eickhoff, D.P., Kaiser, J.S., Hill, R.J., & Spaw, J.M. (2013). Massive Cretaceous-Paleogene boundary deposit, deep-water Gulf of Mexico: New evidence for widespread Chicxulub-induced slope failure: *Geology, 42(*9), 983-986, https://doi.org/10.1130/G34503.1

Dinarès-Turella, J., Westerhold, T., Pujaltec, V., Röhl, U., & Kroon, D. (2014). Astronomical calibration of the Danian stage (Early Paleocene) revisited: settling chronologies of sedimentary records across the Atlantic and Pacific Oceans: *Earth and Planetary Science Letters,405*, 119–131.

Duncombe, J. (2022). The surprising reach of Tonga's giant atmospheric waves. *Eos*, 103, https://doi.org/10.1029/2022EO220050. Published on 21 January 2022.

Expedition 342 Scientists. (2012). Paleogene Newfoundland sediment drifts. *Integrated Ocean Drilling Program, Preliminary Report, 342*. https://doi.org/10.2204/iodp.pr.342.2012

Gisler, G., Weaver, R., & Gittings, M. (2011). Calculations of asteroid impacts into deep and shallow water. *Pure and Applied Geophysics*, 168, 1187-1198, https://doi.org/10.1007/s00024-010-0225-7

Glimsdal, S., Pedersen, G.K., Langtangen, H.P., Shuvalov, V., and Dypvik, H. (2007). Tsunami generation and propagation from the Mjølnir asteroid impact. *Meteoritics & Planetary Science,* 42, 1473-1493. https://doi.org/10.1111/j.1945-5100.2007.tb00586.x

Gulick, S.P.S., Barton, P.J., Christeson, G.L., Morgan, J.V., McDonald, M., Mendoza-Cervantes, K.,Pearson, Z.F., Surendra, A., Urrita-Fucugauchi, J., Vermeesch, P.M., & Warner, M.R. (2008).

Importance of pre-impact crustal structure for the asymmetry of the Chicxulub impact crater. *Nature Geoscience*, 1, 131-135, https://doi.org/10.1038/ngeo103

Gulick, S., Morgan, J., and Mellett, C.L. (2016). *Expedition 364 Scientific Prospectus: Chicxulub: drilling the K-Pg impact crater.* International Ocean Discovery Program. https://doi.org/10.14379/iodp.sp.364.2016

Hines, B.R., Kulhanek, B.K., Holls, C.J., Atkins, C.B., & H E G Morgans, H.E.G., (2013). Paleocene–Eocene Stratigraphy and Paleoenvironment at Tora, Southeast Wairarapa, New Zealand, New Zealand Journal of Geology and Geophysics, https://doi.org/10.1080/00288306.2013.836112

Hollis, C. J. (2003). The Cretaceous/Tertiary boundary event in New Zealand: profiling mass extinction. *New Zealand: Journal of Geology and Geophysics, 46*, 307-321.

Husson, D., GalbrunB., Laskar , J., Hinnov, l.A., Thibault, N., Gardin, S., and Locklair, R.E. (2011). Astronomical calibration of the Maastrichtian (Late Cretaceous): *Earth and Planetary Science Letters, 128,* 128-340.

International Geologic Congress, (1989). 28th International Geological Congress, Washington, D.C, July 9- 19,624 p., doi 10.1016/0045-8732(88)90022-1

Keller, G. (1988). Extinction, survivorship and evolution of planktic foraminifers across the Cretaceous/Tertiary boundary at El Kef, Tunisia. *Marine Micropaleontology, 13,* 239-263.

Keller, G., & Lindinger, M. (1989). Stable isotope, TOC and CaCO3 record across the Cretaceous/Tertiary boundary at El Kef, Tunisia. *Palaeogeography, Palaeoclimatology, Palaeoecology, 73*, 243-265.

Keller, G., Lopez-Oliva, J.G., Stinnesbeck, W., & Adatte, T. (1997). Age, stratigraphy, and deposition of near-K/T siliciclastic deposits in Mexico: Relation to bolide impact. *Geological Society of America Bulletin, 109*, 410–428.

Keller, G., Adatte, T., Berner, Z., Harting, M., Baum, G., Prauss, M.. Tantawy, A., & Stueben, D. (2007). Chicxulub impact predates K–T boundary: New evidence from Brazos, Texas. *Earth and Planetary Science Letters, 255*, 339-356.

Kiessling, W., & Claeys, P. (2001). A geographic database approach to the KT boundary, In E. Buffetaut & C. Koeberl (Eds.) *Geological and biological effects of impact events*. (Berlin, Springer), 83−140.

Kinsland, G.L., Egedahl, K., Strong, M.A., & Ivy, R. (2021). Chicxulub impact tsunami megaripples in the subsurface of Louisiana: Imaged in petroleum industry seismic data. *Earth and Planetary Science Letters,* 570, 007063, https://doi.org/10.1016/j.epsl.2021.117063

Kirby, J.T. (2016). Boussinesq models and their application to coastal processes across a wide range of scales. Journal of Waterway, Port, Coastal and Ocean Engineering, 142(6), 03116004, https://doi.org/10.1061/(ASCE)WW.1943-5460.0000350

Kodama, K., Fukuoka, M., Aita, Y., Sakai, T., Hori, R.S.,Takemura, A., Campbell, H.J., Hollis, C.J., Grant-Mackie, J.A., and Spörli, K.B., 2007, Paleomagnetic results from Arrow Rocks in the framework of paleomagnetism in pre-Neogene rocks from New Zealand, in Spörli, in K.B., Takemura, A., and Hori, R.S., (Eds.) The Oceanic Permian/Triassic Boundary Sequence at Arrow Rocks

(Oruatemanu), Northland, New Zealand: Lower Hutt, New Zeland, *Geological and Nuclear Science Monograph 24*, 177–196.

Kunkel, C.M., Hallberg, R.W., & Oppenheimer, M. (2006). Coral reefs reduce tsunami impact in model simulations, Geophysical Research Letters 33, L23612, https://doi.org/10.1029/2006GL027892.

Laird, M.G., Bassett, K. N., Schiøler , P., Morgans, H. E. G, Bradshaw, J. D. & Weaver, S.D. (2003). Paleoenvironmental and tectonic changes across the Cretaceous/Tertiary boundary at Tora, southeast Wairarapa, New Zealand: A link between Marlborough and Hawke's Bay. *New New Zealand Journal of Geology and Geophysical, 46,* 275-293.

Laskar, J., Fienga, A., Gastineau, M., and Manche, H. (2011). La2010: a new orbital solution for the long-term motion of the Earth. *Astronomy and Astrophysics, 532*, A89. http://dx.doi.org/10.1051/0004-6361/201116836.

Lonsdale, P., & Southard, J. B. (1974). Experimental erosion of north pacific red clay: Marine *Geology, 17,* M51– *M60.*

Lowrie, W., & Alvarez, W. (1977). Upper Cretaceous-Paleocene magnetic stratigraphy at Gubbio, Italy. III. Upper Cretaceous magnetic stratigraphy. *Geological Society of America Bulletin, 88*, 374-377.

MacLeod, K.G., Whitney, D.L., Huber, B. T., & Koeberl, C. (2007). Impact and extinction in remarkably complete Cretaceous-Tertiary boundary sections from Demerara Rise, tropical western North Atlantic. *Geological Society of America Bulletin, v.119* (1/2), 101–115;. doi:10.1130/B25955.1.

MacLeod, K.G., Quinton, P.C., Sepúlveda, J. & Negra, M.H. (2018). Postimpact earliest Paleogene warming shown by fish debris oxygen isotopes (El Kef, Tunisia). *Science, 360,* 1467–1469.

Margolis, S.V., Mount, J.F. & Doehne, E. (1987). The Cretaceous/Tertiary boundary carbon and oxygen isotope stratigraphy, diagenesis, and paleoceanography at Zumaya, Spain: *Paleoceanography, 2* (4), 361-377.

Matsui, T., Imamura, F., Tajika, E., Nakano, Y., & Fujisawa, Y. (2002). Generation and propagation of a tsunami from the Cretaceous-Tertiary impact event. *Catastrophic Events and Mass Extinctions: Impacts and Beyond*, (356), 69–77. https://doi.org/10.1130/0-8137-2356-6.69.

Matsuyama, M., Ikeno, M., Sakakiyama, T., Takeda, T. (2007). A study of tsunami wave fission in an undistorted experiment. Pure Appl. Geophys. 164, 617–631. DOI 10.1007/s00024-006-0177-0

Maurrasse, F. J.-M. R., and Sen, G. (1991). Impacts, tsunamis and the Haitian Cretaceous-Tertiary boundary layer. *Science, 252*, 1690–1693.

McCave, I.N. (1984). Erosion, transport and deposition of fine-grained marine sediments. *Fine-Grai Sediments; Deep-Water Processes and Facies*, 15(1), 35–69. https://doi.org/10.1144/GSL.SP.1984.015.01.03

Montanari, A., Claeys, P., Asaro, F., Bermudez, J., & Smit, J. (1994). Preliminary stratigraphy and iridium and other geochemical anomalies across the KT boundary in the Bochil Section (Chiapas, southeastern Mexico), in New developments regarding the K/T event and other catastrophes in Earth history. *Lunar and Planetary Institute Contribution 825*, 84–85.

Morgan, J., Artemieva, N., & Goldin, T. (2013). Revisiting wildfires at the K-Pg boundary. *Journal of Geophysical Research: Biogeosciences*, *118*(4), 1508–1520. https://doi.org/10.1002/2013JG002428

Morgan, J.V, Gulick, S.P.S., Bralower, T., Chenot, E., Christeson, G., Claeys, P., et al. (2016). The formation of peak rings in large impact craters. Science, 354(6314), 878–882, https://doi.org/10.1126/science.aah6561

Müller, R.D., Sdrolias, M., Gaina, C., Steinberger, B., & Heine, C. (2008). Long-term sea-level fluctuations driven by ocean basin dynamics. Science 319, 1357-1362, https://doi.org/10.1126/science.1151540.

Pardo, A., Ortiz, N. & Keller, G. (1996). Latest Maastrichtian foraminiferal turnover and its environmental implications at Agost, Spain. In: In N. Macleod & G. Keller (Eds.), *The Cretaceous/Tertiary Boundary Mass Extinction: Biotic and Environmental Events*. (Norton, New York), 139-171.

Pedersen, G. (2008). Modeling runup with depth integrated equation models. In: L-F Liu, H. Yeg, C. Synolakis (Eds.),Advanced Numerical Models for Simulating Tsunami Waves and Runup, World Scientific, 3-41, https://doi.org/10.1142/6226

Robertson, D., Pokorný, P., Granvik, M., Wheeler, L., & Rumpf, C. (2021). Latitude variation of flux and impact angle of asteroid collisions with earth and the moon. *Planetary Science Journal,* 2, 88. https://doi.org/10.3847/PSJ/abefda

Rudnick, D. L., et al. (2003), From tides to mixing along the Hawaiian Ridge, *Science, 301*(5631), 355–357. https://doi.org/10.1126/science.1085837

Sanford, J. C., Snedden, J.W., & Gulick, S.P.S. (2016). The Cretaceous-Paleogene boundary deposit in the Gulf of Mexico: Large-scale oceanic basin response to the Chicxulub impact. *Journal of Geophysical Research, Solid Earth, v. 121 (3)*, 1240-1261. https://doi.org/10.1002/2015JB012615

Schroeder, W. (1984). The empirical age-depth relation and depth anomalies in the Pacific Ocean Basin. Journal of Geophysical Research 89, 9873-9883, https://doi.org/10.1029/JB089iB12p09873.

Schulte, P., Alegret, L., Arenillas, I., Arz, J. A., Barton, P. J., Bown, P. R., et al. (2010). The Chicxulub asteroid impact and mass extinction at the Cretaceous-Paleogene boundary. *Science (New York, N.Y.)*, *327*(5970), 1214–1218, https://doi.org/10.1126/science.1177265

Schulte, P., Speijer, R., Mai, H., & Kontny, A. (2006). The Cretaceous–Paleogene (K–P) boundary at Brazos, Texas: Sequence stratigraphy, depositional events and the Chicxulub 903 impact. *Sedimentary Geology,* 184, 77-109.

Schulte, P., Speijer, P., Brinkhuis , H., Kontny, A., Claeys, P., Galeotti , S., & Smit, J. (2008). Comment on the paper "Chicxulub impact predates K–T boundary: New evidence from Brazos, Texas" by Keller et al., 2008: Earth and Planetary Science Letters, 269, 614-620.

Scotese, C. R. (1997). *The PALEOMAP Project: paleogeographic atlas and plate tectonic software.* https://cmr.earthdata.nasa.gov/search/concepts/C1214607516-SCIOPS

Sissingh, W. (1977). Biostratigraphy of Cretaceous calcareous nannoplankton. *Geologie en Mijnbouw, v. 56*(1), 37-65.

Smit, J., Roep, T.B., Alvarez, W., Montanari, A., Claeys, P., Grajales-Nishimura, J.M., & Bermudez, J. (1996). Coarse-grained, clastic sandstone complex at the K/T boundary around the Gulf of Mexico: Deposition by tsunami waves induced by the Chicxulub impact. *Geological Society of America Special Paper 307*, 151−182.

Smith, W.H.F., Scharroo, R., Titov, V.V., Arcas, D., & Arbic, B.K. (2005). Satellite Altimeters Measure Tsunami—Early Model Estimates Confirmed. *Oceanography*, *18*(2), 11–13. https://doi.org/10.5670/oceanog.2005.62.

Smith, W.H.F., & Sandwell, D.T. (1997). Global seafloor topography from satellite altimetry and ship depth soundings. *Science*, 277, 1956-1962. https://doi.org/10.1126/science.277.5334.1956.

Son, S., Lynett, P. & Kim, D.-H. (2011). Nested and multi-physics modeling of tsunami evolution from generation to inundation. Ocean Modelling 38(1), 96-113. https://doi.org/10.1016/j.ocemod.2011.02.007.

Stinnesbeck, W., Keller, G., de la Cruz, J., de León, C., MacLeod, N., & Whittaker, J.E. (1997). The Cretaceous–Tertiary transition in Guatemala: limestone breccia deposits from the South Peten basin. *Geologische Rundschau, 86*, 686-709.

Synolakis, C.E., Bernard, E.N., Titov, V.V., Kânoğlu, U., & González, F.I. (2008). Validation and verification of tsunami numerical models. *Pure and Applied Geophysics,* 165, 2197–2228. https://doi.org/10.1007/s00024-004-0427-y.

Tang, L., et al. (2012), Direct energy estimation of the 2011 Japan tsunami using deep-ocean pressure measurements, *Journal of Geophysical Research,* 117, C08008, https://doi.org/10.1029/2011JC007635

Titov, V.V., & Synolakis, C.E. (1995) Modeling of breaking and nonbreaking long-wave evolution and runup using VTCS–2. *Journal of Waterway, Port, Coastal and Ocean Engineering*, 121, 308-316, https://doi.org/10.1061/(ASCE)0733-950X(1995)121:6(308)

Titov, V.V., Kânoğlu, U., & Synolakis, C. (2016): Development of MOST for real-time tsunami forecasting. *Journal of Waterway, Port, Coastal and Ocean Engineering*, 142(6), 03116004, https://doi.org/10.1061/(ASCE)WW.1943-5460.0000357

Titov, V.V., Rabinovich, A.B., Mofjeld, H.O., Thomson, R.E., & González, F.I. (2005): The global reach of the 26 December 2004 Sumatra Tsunami. *Science*, *309*(5743), 2045–2048, https://doi.org/10.1126/science.1114576

Toon, O.B., Pollack, J.B., Ackerman, T.P., Turco, R.P., McKay, C.P., and Liu, M.S. (1982). Evolution of an impact-generated dust cloud and its effects on the atmosphere. In L. T. Silver, and P. H. Schultz, (Eds.), Geological implications of impacts of large asteroids and comets on Earth. *Geological Society of America Special Paper 190,* 187–200.

Van Dorn, W.G., Le Méhauté, B., Hwang. L.-S. (1968). Handbook of explosion-generated water waves. Report TC-130. Tetra Tech Inc., Pasadena, CA.

Ward, S. (2012), Chicxulub Tsunami.mov, *YouTube*. Available from: https://www.youtube.com/watch?v=Dcp0JhwNgmE

Ward, S. (2021), Chicxulub Tsunami-2.mov, *YouTube*. Available from: https://www.youtube.com/watch?v=5qhqmXMUu6U&t=31s

Weiss, R., Wünnemann, K., & Bahlburg, H. (2006). Numerical modelling of generation, propagation and run-up of tsunamis caused by oceanic impacts: model strategy and technical solutions. *Geophysical Journal International*, 167, 77-88. https://doi.org/10.1111/j.1365-246X.2006.02889.x

Weiss, R., and Wünnemann, K. (2007). Large waves caused by oceanic impacts of meteorites. In Tsunami and Nonlinear Waves (pp. 237-261). Springer, Berlin, Heidelberg.

Wünnemann, K., Collins, G. S., and Weiss, R. (2010). Impact of a cosmic body into Earth's ocean and the generation of large tsunami waves: insight from numerical modeling. *Reviews of Geophysics,* 48, RG4006, https://doi.org/10.1029/2009RG000308

Westerhold, T., Röhl, U., and Laskar, J. (2012). Time scale controversy: accurate orbital calibration of the Early Paleogene. *Geochemistry, Geophysics, Geosystems,*13, 73-82. http://dx.doi.org/10.1029/2012gc004096.

Wünnemann, K., & Weiss, R. (2015). The meteorite impact-induced tsunami hazard. *Philosophical Transactions of the Royal Society A: Mathematical, Physical and Engineering Sciences*, *373*(2053). https://doi.org/10.1098/rsta.2014.0381

Wünnemann, K., Collins, G.S., & Melosh, H.J. (2006). A strain-based porosity model for use in hydrocode simulations of impacts and implications for transient crater growth in porous targets. *Icarus*, *180*(2), 514–527. https://doi.org/10.1016/j.icarus.2005.10.013

Wunsch, C., & R. Ferrari (2004), Vertical mixing, energy, and the general circulation of the oceans, *Annual Reviews of Fluid Mechanics, 36*, 281–314.

Zhou, H., Wei, Y., & Titov, V.V. (2012): Dispersive modeling of the 2009 Samoa tsunami. *Geophysical Research Letters*, 39, L16603, https://doi.org/1029/2012GL053068

References in Supplementary Tables ST-1 and ST-2

Abramovich, S., Keller, G., Adatte, T., Stinnesbeck, W., Hottinger, L., Stüben, D., Berner, Z., Ramanivosoa,B. & Randriamanantenasoa, A. (2002). Age and paleoenvironment of the Maastrichtian-Paleocene of the Mahajanga Basin, Madagascar: a multidisciplinary approach. *Marine Micropaleontology 47*, 17–70. http://dx.doi.org/10.1016/S0377- 8398(02)00094-4.FIX DOI; should be clickable

Açıkalın, S, Vellekoop, J., Ocakoglu, F., Yılmaz, I.Ö., Smit, J., Altıner, S. Ö., Goderis, S, Vonhof, H., Speijer, R.P., Woelders, L., Fornaciari, E., & Brinkhuis, H. (2015). Geochemical and palaeontological characterization of a new K-Pg Boundary locality from the Northern branch of the Neo-Tethys:

Mudurnu e Göynük Basin, NW Turkey: *Cretaceous Research, 52,* 251-267.

Adatte, T., Keller, G., Burns, S., Stoykova, K.H., Ivanov, M.I., Vangelov, D., Kramar, U., & Stüben, D. (2016). Paleoenvironment across the Cretaceous-Tertiary transition in eastern Bulgaria: *Geological Society of America Special Paper 356*, 231-251.

Alegret, L., Arenillas, I., Diaz, C., Grajales-Nishimura, J., Meléndez, A., Molina, E., Rojas Museo , R., & Soria, A.R. (2005). Cretaceous-Paleogene boundary deposits at Loma Capiro, central Cuba: Evidence for the Chicxulub impact. *Geology, 33* (9), 721-724.

Alegret, L., Thomas, E, & Lohmann, K.C. (2012). End-Cretaceous marine mass extinction not caused by productivity collapse. P*roceedings of the National Academy of Sciences of the United States of America 109*(3), 728-732.

Alegret, L., Kaminski, M.A., & Molina, E. (2004). Paleoenvironmental recovery after the Cretaceous/Paleogene boundary crisis: evidence From the marine Bidart section (SW France). *Palaios,, 19,* 574-586.

Alvarez, W., Asaro, F. & Montanari, A. (1990). Iridium profile for 10 million years across the Cretaceous-Tertiary Boundary at Gubbio (Italy). *Science, 250*, 1700-1702.

Alvarez, W. & Lowrie, W. (1979). Upper Cretaceous palaeomagnetic stratigraphy at Moria,Umbrian Apennines, Italy: verification of the Gubbio section: *Geophysical Journal of the Royal Astronomical. Society, 57*, 1-17.

Andrews, J.E., Packham, G., et al. (1975). *Initial Reports of the Deep Sea Drilling Project, Volume 30*. Washington DC: U.S. Govt. Printing Office.

Arncth, J.-D, Matzigkcit, U., & Boos, A. (1985). Carbon isotope geochemistry of the Cretaceous-Tertiary section of the Wasserfallgraben, Lattengebirge, southeast Germany. *Earth and Planetary Science Letters, 75*, 50-58.

Askin, R. A. (1985). The palynological record across the Cretaceous/Tertiary transition on Seymour Island, Antarctica. In R.M. Feldmann, M.O. Woodburne, (Eds.), *Geology and paleontology of Seymour Island: Geological Society of America Memoir 169*, (pp. 155-162).

Austin, J. A., Jr., Schlager, W., Palmer, A.A. et al. (1986). *Proceedings of the Ocean Drilling Program, Initial Reports. (Pt. A), 101.* College Station, TX: Ocean Drilling Program.

Barker, P. F., Dalziel, I.W.D., et al. (1976). *Initial Reports of the Deep Sea Drilling Project 36*. Washington DC: U.S. Govt. Printing Office.

Barker, P. F., Carlson, R.L., & Johnson, D.A. (1983). *Initial Reports Deep Sea Drilling Program, 72*. Washington DC: U.S. Govt. Printing Office.

Barker, P. F., Kennett, J.P., et al. (1988). *Proceedings of the Ocean Drilling Program, Initial Reports, 113*. College Station, TX: Ocean Drilling Program.

Barker, P. F, Kennett, J.P., et al. (1990), *Proceedings of the Ocean Drilling Program, Scientific Results,* *113*. College Station, TX: Ocean Drilling Program.

Barrera, E. (1994). Global environmental changes preceding the Cretaceous-Tertiary boundary: Early-late Maastrichtian transition: *Geology, 22*, 877-880,

Barron, J., Larsen, B., et al.. 1989, *Proceedings of the Ocean Drilling Program, Initial Reports, 119*. College Station, TX: Ocean Drilling Program.

Benson, W. E., Sheridan, R. E., et al. (1978). *Initial Reports of the Deep Sea Drilling Project, 44*.Washington DC: U.S. Govt. Printing Office), 1005 pp.

Bleil, U., (2007). The magnetostratigraphy of northwest Pacific sediments, Deep Sea Drilling Project Leg 86.In G. R.Heath, L. H.Burckle et al., *Initial Reports of the Deep Sea Drilling Project, 86*. Washington DC: U.S. Govt. Printing Office.

Boillot, G., Winterer, E.L., Meyer, A.W., et al. (1987). *Proceedings of the Ocean Drilling Program, Initial Reports, (Pt. A) 103*. College Station, TX: Ocean Drilling Program.

Bolli, H. M., Ryan, W.B.F. et al. (1978 *Initial Reports of the Deep Sea Drilling Project, Volume 40*. Washington DC: U.S. Govt. Printing Office.

Bowles, J. (2007). Data report: revised magnetostratigraphy and magnetic mineralogy of sediments from Walvis Ridge, Leg 208 In D. Kroon, D., J.C. Zachos, C. Richter. (Eds.): *Proceedings of the Ocean Drilling Program, Scientific Results, 208.* (College Station, TX: Ocean Drilling Program), 24 pp. doi:10.2973/odp.proc.sr.208.2007 .

Bowman, V.C., Francis, J.E., Askinb, R.A., Riding, J.B., & Swindles, G.T. (2014, Latest Cretaceous–earliest Paleogene vegetation and climate change at the high southern latitudes: palynological evidence from Seymour Island, Antarctic Peninsula.

Bralower, T.J., & Siesser, W.G. (1992). Cretaceous calcareous nannofossil biostratigraphy of Sites 761, 762, and 763, Exmouth and Wombat Plateaus, Northwest Australia. In U. von Rad, B.U. Haq, et al.: *Proceedings of the Ocean Drilling Program, Initial Reports, 122*. College Station, TX, Ocean Drilling Program.

Bralower, T.J., Premoli Silva, I., Malone, M.J. et al. (2002a). Proceedings of the Ocean Drilling Program, Initial Reports, (Pt. A), 198. College Station, TX: Ocean Drilling Program. doi:10.2973/odp.proc.ir.198.2002,

Bralower, T.J., Premoli Silva, I., & Malone, M.J. (2002b). Leg 198 synthesis: a remarkable 120 M.Y. record of climate and ceoanography from Shatsky Rise, Northwest Pacific Ocean, In T.J. Bralower, I. Premoli Silva, M.J. Malone, et al. *Proceedings of the Ocean Drilling Program, Initial Reports, 198.* College Station, TX: Ocean Drilling Program. doi:10.2973/odp.proc.ir.198.2002, p. 1-47.

Brinkhuis, H. & Zachariasse, W.J. (1988). Dinoflagellate cysts, sea level changes and planktonic foraminifers across the Cretaceous-Tertiary boundary at El Haria, Northwest Tunisia. *Marine Micropaleontology, 13*, 153-191.

Buffler, R. T., Schlager, W. et al. (1984). *Initial Reports of the Deep Sea Drilling Project, 11*.

Washington DC: U.S. Govt. Printing Office.

Burns, R. E., Andrews, J.E. et al. (1973). *Initial Reports of the Deep Sea Drilling Project, 21*. Washington DC: U.S. Govt. Printing Office.

Carter, R.M., McCave, I.N., Richter, C., Carter, L., et al. (1999). Proceedings of the Ocean Drilling Program, Initial Reports, 181 [Online]. doi:10.2973/odp.proc.ir.181.2000, Available from World Wide Web: <http://www-odp.tamu.edu/publications/181_IR/181ir.htm>.

Clemens, S.C., Kuhnt, W., LeVay, L.J., & the Expedition 353 Scientists. (2015). *Expedition 353 Preliminary Report: Indian Monsoon Rainfall*. International Ocean Discovery Program. http://dx.doi.org/10.14379/iodp.pr.353.2015.

Ciesielski, P. F., Kristoffersen, Y. et al. (1988). *Proceedings of the Ocean Drilling Program, Initial Reports*, *114*. College Station, TX: Ocean Drilling Program.

Coffin, M.F., Frey, F.A., Wallace, P.J. et al. (2000). *Proceedings of the Ocean Drilling Program, Initial Reports, 183* [Online]. doi:10.2973/odp.proc.ir.183.2000, Available from World Wide Web: <http://www-odp.tamu.edu/publications/183_IR/183ir.htm>.

Creager, J. S., Scholl, D.W. et al. (197). *Initial Reports of the Deep Sea Drilling Project.*Washington DC: U.S. Govt. Printing Office), 930 pp.

Davies, T. A., Luyendyk, B.P. et al. (1974). *Initial Reports of the Deep Sea Drilling Project, 26*. Washington DC: U.S. Govt. Printing Office.

Dinarès-Turell, J., Westerhold, T., Victoriano Pujalte, V., Röhl, U. & Kroon, D. (2013). Settling the Danian astronomical time scale: a prospective global unit stratotype at Zumaia, Basque Basin. In R. Rocha et al., (Eds), *STRATI 2013*. Springer International Publishing Switzerland. doi: 10.1007/978-3-319-04364-7_38

Donovan, A.D., Baum, G.R., Blechschmidt, G.L., Loutit, T.S., Pflum, C.E. & Vail, P.R. (2012). Sequence Stratigraphic Setting of the Cretaceous-Tertiary boundary in central Alabama. In Sea-Level Changes- An Integrated Approach, *SEPM Society for Sedimentary Geology Special Publication* No. 42, 299-307.

Edgar, N. T., Saunders, J.B. et al. (1973). *Initial Reports of the Deep Sea Drilling Project, 15.*Washington DC: U.S. Govt. Printing Office.

Elliot . D.H., Askin, R.A., Kyte, F.T, & Zinsmeister, W. J. (1994). Iridium and dinocysts at the Cretaceous-Tertiary boundary on Seymour Island, Antarctica: Implications for the K-T event: *Geology, 22,* 675-678.

Erbacher, J., Mosher, D.C., Malone, M.J. et al. (2004). *Proceedings of the Ocean Drilling Program, Initial Reports, 207*. College Station, TX: Ocean Drilling Program. doi:10.2973/odp.proc.ir.207.2004.

Esmeray-Senlet, S., Wright, J.D., Olsson, R.K., Miller, K.G., Browning, J.V. & Quan, T.M. (2015). Evidence for reduced export productivity following the Cretaceous/Paleogene mass extinction: *Paleoceanography, 30*, 718–738. doi:10.1002/2014PA002724.

Exon, N.F., Kennett, J.P., & Malone, M.J. (2004). Leg 189 synthesis: Cretaceous–Holocene history of the Tasmanian Gateway. In N.F. Exon, J.P. Kennett, and M.J. Malone, (Eds.). *Proceedings of the Ocean Drilling Program, Scientific Results, 189*, 1-37. College Station, TX: Ocean Drilling Program. doi:10.2973/odp.proc.sr.189.101.2004

Galburn, B. (1992). Magnetostratigraphy of Upper Cretaceous and Lower Tertiary sediments, Sites 761 and 762, Exmouth Plateau, Northwest Australia. In U. von Rad, B.U. Haq, et al. *Proceedings of the Ocean Drilling Program, Scientific. Results, 122*: College Station, TX: Ocean Drilling Program.

Galbrun, B., and Gardin, S. (2004). New chronostratigraphy of the Cretaceous–Paleogene boundary interval at Bidart, France: *Earth and Planetary Science Letters, 224*, 19-32.

Graciansky, P. C. de, Poag, C.W. et al. (1985). *Initial Reports of the Deep Sea Drilling Project, 80*. Washington DC: U.S. Govt. Printing Office.

Hailwood, E.A. & Clement, B.M. (1991). Magnetostratigraphy of Sites 699 and 700, East Georgia Basin. In P. F. Ciesielski, Y. Kristoffersen, et al. *Proceedings of the Ocean Drilling Program, Scientific Results, 114.* College Station, TX: Ocean Drilling Program. 337-357.

Hamilton, N. (1990). Mesozoic magnetostratigraphy of Maud Rise, Antarctica, In P.F. Barker, J.P. Kennett, et al. *Proceedings of the Ocean Drilling Program, Scientific Results, 113*. College Station, TX: Ocean Drilling Program.

Hamilton, N. & Suzyumov, A. E. (1983). Late Cretaceous magnetostratigraphy of Site 516, Rio Grande Rise, southwestern Atlantic Ocean, Deep Sea Drilling Project, Leg 72. In P.F. Barker, R.L. Carlson, and D.A. Johnson: *Initial Reports of the Deep Sea Drilling Project, 72*. Washington DC: U.S. Govt. Printing Office, 723-730.

Hansen. J. M. (1979). Dinoflagellate zonation around the boundary. In T. Birkelund, & R. G. Bromley, (Eds.). *Cretaceous-Tertiary boundary events. Volume I*. (University of Copenhagen, Denmark), 136-141.

Hansen, H.J., Drobne, K., & Gwozdz, R. (1995). The K/T boundary in Slovenia: Dating by magnetic susceptibility and an iridium anomaly in a debris flow: 4th Int. workshop European Science Network "Impact Cratering and Evolution of Planet Earth",Ancona, May 1995, Abstracts and Field Trips. (Università degli Studi Urbino, Ancona) 84–85.

Haq, B.U., von Rad, U., O'Connell, S. et al., (1990). *Proceedings of the Ocean Drilling Program, Initial Reports, 122.* College Station, T X: Ocean Drilling Program).

Hart, M.B., Feist, S.E., Håkanssonc, E., Heinbergd, C., Price, G.D., Lenge, M.J., & Watkinson, M. P. (2005). The Cretaceous–Palaeogene boundary succession at Stevns Klint, Denmark: Foraminifers and stable isotope stratigraphy: *Palaeogeography, Palaeoclimatology, Palaeoecology*, 224), 6 – 26.

Hay, W. W., Sibuet, J.-C. et al. (1984). *Initial Reports of the Deep Sea Drilling Project,75*. Washington DC: U.S. Govt. Printing Office.

Hayes, D. E., Pimm, A.C. et al. (1972). *Initial Reports of the Deep Sea Drilling Project, 14*. Washington DC: U.S. Government Printing Office.

Hayes, D. E., Frakes, L.A. et al. (975). *Initial Reports of the Deep Sea Drilling Project, 28.* Washington DC: U.S. Govt. Printing Office.

Heath, G. R., Burckle, L.H. et al. (1985). *Initial Reports of the Deep Sea Drilling Project, 86*. Washington DC: U.S. Govt. Printing Office.

Herbert, T.D. & D'Hondt, S.L. (1990). Precessional climate cyclicity in Late Cretaceous-Early Tertiary marine sediments: a high resolution chronometer of Cretaceous-Tertiary boundary events. *Earth and Planetary Science Letters, 99*, 263-275.

Hinz, K., Winterer, E.L. et al. (1984). *Initial Reports of the Deep Sea Drilling Project, 79*. Washington DC: U.S. Govt. Printing Office.

Hollis, C.J. (2002). Biostratigraphy and paleoceanographic significance of Paleocene radiolarians from offshore eastern New Zealand. *Marine Micropaleontology, 46*, 265-316.

Hollis, C. J. , Strong , C. P., Rodgers, K. A., & Rogers, K. M. (2003). Paleoenvironmental changes across the Cretaceous/Tertiary boundary at Flaxbourne River and Woodside Creek, eastern Marlborough: New Zealand. *New Zealand Journal of Geology and Geophysics, 46*, 177-197.

Hollister, C. D., Craddock, C. et al. (1976). *Initial Reports of the Deep Sea Drilling Project, 35*. Washington DC: U.S. Government Printing Office.

Hsü, K. J., and LaBrecque, J.L. et al. (1984). *Initial Reports of the Deep Sea Drilling Project, 73*. Washington (U.S. Govt. Printing Office.

Huber, B.T., Liu, C., Olsson, R.K. & Berggren, W.A. (1994). Comment on "The Cretaceous-Tertiary boundary transition in the Antarctic Ocean and its global implications", by G. Keller: *Marine Micropaleontology, 24*, 91-99.

Keller, G., Adatte, T. , Stinnesbeck, W., Stüben, D., Kramar, U., Berner, Z., Li, L., & Perch-Nielsen, K. v. S. (1998). The Cretaceous-Tertiary transition on the shallow Saharan Platform of Southern Tunisia. *Geobios, 30,* 951-975.

Keller, G., Adatte, T., Tantawy, A.A., Berner, Z., Stüben, D. (2007). High stress late Cretaceous to early Danian paleoenvironment in the Neuquen Basin, Argentina. *Cretaceous Research, 28*, 939–960. http://dx.doi.org/10.1016/j.cretres.2007.01.006.

Keller, G., Khozyem, H.M., Adatte, T., Malarkodi, N., Spangenberg, J.E., Stinnesbeck, W. (2013,). Chicxulub impact spherules in the North Atlantic and Caribbean: age constraints and Cretaceous-Tertiary boundary hiatus. *Geological Magazine 150*, 885–907. http://dx.doi.org/10.1017/S0016756812001069.

Kroenke, L. W., Berger, W.H., Janecek, T.R. et al. (1991). *Proceedings of the Ocean Drilling Program, Initial Report,130*. College Station, TX: Ocean Drilling Program.

Kyte, F.T., Smit, J. & Wasson,J.T. (1985). Siderophile interelement variations in the Cretaceous-Tertiary boundary sediments from Caravaca, Spain. *Earth and Planetary Science Letters, 73,* 183-195.

Lancelot, Y., Winterer, E.L. (1980). *Initial Reports of the Deep Sea Drilling Project, 50.* Washington DC: U.S. Government Printing Office.

Lancelot, Y., Seibold, E. et al. (1977). *Initial Reports of the Deep Sea Drilling Project, 41.* Washington DC: U.S. Government Printing Office.

Landman, N.H., Johnson, R.O., Garb, M.P., Edwards, L.E., & Kyte, F.T. (2007). Tertiary boundary interval on the Atlantic coastal plain, with a description uf the highest ammonite zones in North America. Part III. Manasquan River Basin, Monmouth County, New Jersey. *Bulletin of the American Museum Natural History, 30*, 122 pp.

Larson, R. L., Moberly, R. et al. (1975). *Initial Reports of the Deep Sea Drilling Project, 32*. Washington DC: U.S. Government Printing Office.

Latal, C. (2004). The Cretaceous-Paleogene boundary section of Gorgo a Cerbara: an integrated stratigraphical study. *Annals Naturhistorisches Museum Wien, 160A,* 259-279.

Ludwig, W. J., Krasheninikov, V.A. et al. (1983). *Initial Reports of the Deep Sea Drilling Project, 71*. Washington DC: U.S. Government Printing Office.

MacLeod, K.G.& Keller, G. (1991a). How complete are Cretaceous/Tertiary boundary sections? A chronostratigraphic estimate based on graphic correlation. *Geological Society of America Bulletin, 103*, 1439-1457.

MacLeod, K.G.& Keller, G. (1991b). Hiatus distributions and mass extinctions at the Cretaceous/Tertiary boundary. *Geology, 19,* 497-501.

Mahoney, J.J., Fitton, J.G., Wallace, P.J. et al. (2001). *Proceedings of the Ocean Drilling Program, Initial Reports 19.* College Station, TX, Ocean Drilling Program. doi.10.2973/odp.proc.ir.192.2001.

Mateo, P., Keller, G., Adatte. T. & Spangenberg., J.E. (2016). Mass wasting and hiatuses during the Cretaceous-Tertiary transition in the North Atlantic: Relationship to the Chicxulub impact. *Palaeogeography, Palaeoclimatology, Palaeoecolology. 441*, 96–115. http://dx.doi.org/10.1016/j.palaeo.2015.01.019

Mascle, J., Lohmann, G.P., Clift, P.D. et al. (1996). *Proceedings of the Ocean Drilling Program, Initial Reports, 159.* College Station, TX, Ocean Drilling Program.

Maxwell, A. E. et al. (1970). *Initial Reports of the Deep Sea Drilling Project, 3*. Washington DC: U.S. Government Printing Office.

Miller, K.G., Sugarman, P.J., Browning, J.V. et al. (1998). Bass River Site report. *Scientific results, Ocean Drilling Program, Leg 174AX Supplement*, 5-43. College Station, TX: Ocean Drilling Program. 10.2973/odp.proc.ir.174AX.1998

Miller, K.G., Sugarman, P.J., Browning, J.V. et al. (1999). *Proceedings of the Ocean Drilling Program, Initial Reports , 174AX (Suppl.)*. College Station, TX: Ocean Drilling Program. doi:10.2973/Odp.Proc.Ir.174axs.104.1999.

Moberly, R., Schlanger, S.O. et al. (1986). *Initial Reports of the Deep Sea Drilling Project, 89.* Washington DC: U.S. Government Printing Office.

Molina, E., Alegret1, L., Arenillas1, I., Arz1, J.A., Gallala, N., Hardenbol, J., von Salis, K., Steurbaut5, E., Vandenberghe, N. & Zaghbib-Turki, D. (2006). The Global Boundary Stratotype Section and Point for the base of the Danian Stage (Paleocene, Paleogene, "Tertiary", Cenozoic) at El Kef, Tunisia Original definition and revision. *Episodes, 29*(4), 263-273.

Molina, E., Alegret, L., Arenillas, I., and Arz, J. A. (2005). The Cretaceous/Paleogene boundary at the Agost section revisited: paleoenvironmental reconstruction and mass extinction pattern: Journal Iberian *Geolology, 31* (I), 135-150.

Montadert, L., Z, & Roberts, D.G. (1979). *Initial Reports of the Deep Sea Drilling Project, 48.* Washington DC: U.S. Government Printing Office.

Montanari, A., Hay, R.L., Alvarez, W., Asaro, F., Michel, H.V., Alvarez, L.W. & Smit, J. (1983). Spheroids at the Cretaceous-Tertiary boundary are altered impact droplets of basaltic composition: *Geology, 11*, 668-671.

Moore, T. C, Jr., Rabinowitz, P.D. et al. (1984). *Initial Reports of the Deep Sea Drilling Project, 7.* Washington DC: U.S. Government Printing Office.

Michel, H,V., Asaro, F., Alvarez, ,W. Z & Alvarez L.W. (1990,). Geochemical studies of the Cretaceous-Tertiary boundary in ODP holes 689b and 690c. In P.F. Barker, J.P. Kennett, et al: *Proceedings of the Ocean Drilling Program, Scientific Results, 113*. College Station, TX: Ocean Drilling Program, 159-168.

Norris, R.D., Kroon, D., Klaus, A., et al. (1998). *Proceedings of the Ocean Drilling Program, Initial Reports, 171B*. College Station, TX: Ocean Drilling Program.

Ogorelec, B, Dolenec, T., & Drobne, K. (2007). Cretaceous–Tertiary boundary problem on shallow carbonate platform: Carbon and oxygen excursions, biota and microfacies at the K/T boundary sections Dolenja Vas and Sopada in SW Slovenia, Adria CP. *Palaeogeography, Palaeoclimatology, Palaeoecology, 255*, 64–76.

Olsson, R.K., Miller, K.G., Browning, J.V., Wright, J.D., & Cramer, B.S. (2002). Sequence stratigraphy and sea level change across the Cretaceous/Tertiary boundary on the New Jersey passive margin. In C. Koeberl and K.G. MacLeod, K.G., (Eds.) Catastrophic Events and Mass Extinctions: Impacts and Beyond, *Geological Society of America Special Paper 356,* 97–108.

Olsson, R.K., Miller, K.G., Browning, J.V., Habib, D., & Sugarman, P.J. (1997). Ejecta layer at the Cretaceous-Tertiary boundary, Bass River, New Jersey (Ocean Drilling Program Leg 174AX). *Geology, 25*(8),759–762.

Peirce, J., Weissel, J. et al. (1989). *Proceedings of the Ocean Drilling Program, Initial Reports,121.* College Station, TX: Ocean Drilling Program.

Perch Nielsen, K., McKenzie, J., Quziang, H.E., Silver, L.T., & Schultz, P.H. (1982). Biostratigraphy and isotope stratigraphy and the "catastrophic" extinction of calcareous nannoplankton at the

Cretaceous/Tertiary boundary: *Geological Society of America Special Paper, 190,* 353-371.

Poore, R.., Tauxe, L., Percival Jr., S.F., Labrecque, J.L., Wright, R., Petersen, N.Y.P., Smith, C.C., Tucker, P. & Hsu, K.J. (1983). Late Cretaceous-Cenozoic Magnetostratigraphic and biostratigraphic correlations of The South Atlantic Ocean: DSDP Leg 73: *Palaeogeography, Palaeoclimatology, Palaeoecology, 42*, 127-149.

Premoli Silva, I., Haggerty, J., Rack, F. et al. 1993). *Proceedings of the Ocean Drilling Program, Initial Reports, 144*. College Station, TX: Ocean Drilling Program.

Punekar, J., Keller, G., Khozyem, H.M., Adatte, T., Font, E., & Spangenberg, J. (2016). A multi-proxy approach to decode the end-Cretaceous mass extinction: *Palaeogeography, Palaeoclimatology, Palaeoecology, 441*, 116-136.

Rea, D.K., Basov, L.A., Janecek, T.R., Palmer-Julson, A. et al. (1993). *Proceedings of the Ocean Drilling Program, Initial Reports, 145*. College Station, TX: Ocean Drilling Program.

Robin, E., Boclet, D.,, Ph. Bonte, Ph., Froget, L.,, C. Jehanna, C. & Rocchia. R. (1991). The stratigraphic distribution of Ni-rich spinels in Cretaceous-Tertiary boundary rocks at El Kef (Tunisia), Caravaca (Spain) and Hole 761C (Leg 122): *Earth and Planetary Science Letters. V. 107* (3-4), 715-721.

Ruddiman, W., Sarnthein, M., Baldauf, J. et al. (1988). *Proceedings of the Ocean Drilling Program, Initial Reports, 108 (Part A).* College Station, TX: Ocean Drilling Program.

Sager, W.W., Winterer, E.L, Firth, J.V. et al. (1993). *Proceedings of the Ocean Drilling Program, Initial Reports, 14.* College Station, TX, Ocean Drilling Program.

Saito, T., Yamanoi, T., & Kaiho, K. (1986). End-Cretaceous devastation of terrestrial flora in the boreal Far East: *Nature, 323*, 253-255.

Schlanger, S. O., Jackson, E.D. et al.,\ (976). *Initial Reports of the Deep Sea Drilling Project, 33*. Washington DC, U.S. Government Printing Office.

Schlich, R., Wise, Jr., S.W. et al. (1989). *Proceedings of the Ocean Drilling Program, Initial Reports 120*. College Station, TX, Ocean Drilling Program.

Schmitz, B., Keller, G., & Stenvall, O., (1992). Stable isotope and f oraminiferal changes across the Cretaceous-Tertiary boundary at Stevns Klint, Denmark Arguments for long-term oceanic instability before and after bolide-impact event: *Palaeogeography, Palaeoclimatology, Palaeoecology, 96*, 233-260.

Sibuet, J.-C, Ryan, W.B.F., et al. (1979). *Initial Reports of the Deep Sea Drilling Project, 47 Part 2*. Washington DC: U.S. Government Printing Office.

Sigurdsson, H., Leckie, R.M., Acton, G.D., et al. (1997) *Proceedings of the Ocean Drilling Program, Initial Reports, 165*. College Sta- tion, TX: Ocean Drilling Program.

Simpson, E.S.W., Schlich, R., et al. (1974). *Initial Reports of the Deep Sea Drilling Project, 25.* Washington DC: U.S. Government Printing Office.

Smit, J. (1999). The global stratigraphy of the Cretaceous-Tertiary boundary impact ejecta. *Annual Review of Earth and Planetary Sciences, 27*, 75–113.

Smit, J. & Romein, A.J.T. (1985). A sequence of events across the Cretaceous-Tertiary boundary: *Earth and Planetary Science Letters, 74*, 55-170.

Smit, J., Montanari, A., Swinburne, N.H.M., Alvarez, w., Hildebrand, A.R., Margolis, S.V., Claeys, Lowrie, W., & Asaro, , F. (1992). Tektite-bearing, deep-water clastic unit at the Cretaceous-Tertiary boundary in northeastern Mexico: *Geology, 20,* 99-103.

Storms, M.A., Natland, J.H. et al. (1991). *Proceedings of the Ocean Drilling Program, Initial Reports 132*. CollegeStation, TX: Ocean Drilling Program.

Stott, L.D. & Kennett, J. P. (1990). the paleoceanographic and paleoclimatic signature of the Cretaceous/Paleogene boundary in the Antarctic: stable isotopic results from ODP leg 113. In P.F. Barker, J.P. Kennett, et al. *Proceedings of the Ocean Drilling Program, Scientific Results, 113*. College Station, TX: Ocean Drilling Program.

Stüben, D., Kramar, U., Berner, Z., Stinnesbeck, W.. Keller, G.. & Adatte, T. (2002). Trace elements, stable isotopes, and clay mineralogy of the Elles II K/T boundary section in Tunisia: indications for sea level fuctuations and primary productivity. *Palaeogeography, Palaeoclimatology, Palaeoecology, 178*, 321-345.

Suganuma, Y. & Ogg, J. G. (2006). Campanian through Eocene magnetostratigraphy of Sites 1257–1261, OD Leg 207, Demerara Rise (western equatorial Atlantic). In D.C. Mosher, J. Erbacher, and M.J. Malone, (Eds.), *Proceedings of the Ocean Drilling Program, Scientific Results, 207*(3). College Station, TX: Ocean Drilling Program. doi:10.2973/odp.proc.sr.207.102.2006

Supko, P. R., Perch-Nielsen, K. et al. (1977). *Initial Reports of the Deep Sea Drilling Project, 39.* Washington, DC: U.S. Government Printing Office.

Tada, R., Iturralde-Vinent, M.A., Matsui, T., Tajika, E., Oji, T., Goto, K., Nakano, Y., Takayama, H., Yamamoto, S., Kiyokawa, S., Toyoda, K., Garcıa-Delgado, D., Dıaz-Otero, C., & Rojas-Consuegra, R. (2003). K/T boundary deposits in the Paleo-western Caribbean basin. In C. Bartolini, R. T. Buffler, and J. Blickwede, (Eds.), The Circum-Gulf of Mexico and the Caribbean: Hydrocarbon habitats, basin formation, and plate tectonics. *American Association of Petroleum Geologists Memoir 79,* 582–604.

Tarduno, J.A., Duncan, R.A., Scholl, D.W. et al. (2002). *Proceedings of the Ocean Drilling Program, Initial Reports, 197*. College Station, TX: Ocean Drilling Program. doi:10.2973/odp.proc.ir.197.2002

Thiede, J., Vallier, T. L. et al. (1981). *Initial Reports of the Deep Sea Drilling Project, 62*. Washington, DC: U.S. Government Printing Office.

Tobin, S.T., Ward, P. D., Steig, E.J., Olivero, E.B., Hilburn, I.A., Mitchell, R.N., Diamond, M. R., Raub, T.D., & Kirschvink, J. L. (2012). Extinction patterns, δ18 O trends, and magnetostratigraphy from a southern high-latitude Cretaceous–Paleogene section: Links with Deccan volcanism: *Palaeogeography, Palaeoclimatology, Palaeoecology, v. 350–352*, 180 –188.

Tucholke, B. E., Vogt, P.R. et al. (1979). *Initial Reports of the Deep Sea Drilling Project, 43*. Washington, DC: U.S. Government Printing Office.

Tucholke, B.E., Sibuet, J.-C., Klaus, A. et al. (2004). *Proceedings of the Ocean Drilling Program, Scientific Results, 210*. College Station, TX: Ocean Drilling Program. doi:10.2973/odp.proc.ir.210.2004

van Hinte, J. E., Wise, Jr., S.W. et al. (1987). *Initial Reports of the Deep Sea Drilling Project, 93.* Washington, DC: U.S. Government Printing Office.

Veevers, J. J., Heirtzler, J.R. et al. (1974). *Initial Reports of the Deep Sea Drilling Project, 27.* Washington, DC: U.S. Government Printing Office.

von der Borch, C.. Sclater, C.J.G et al. (1974). *Initial Reports of the Deep Sea Drilling Project, 22.* Washington, DC: U.S. Government Printing Office.

von Rad, U., Ryan, W.B.F. et al. (1979). *Initial Reports of the Deep Sea Drilling Project, 47, Part 1*. Washington, DC: U.S. Government Printing Office.

von Rad, U., Haq, B.U. et al. (1992). *Proceedings of the Ocean Drilling Program, Scientific Results*, *122*. CollegeStation, TX: Ocean Drilling Program.

Weissel, J., Peirce, J. , Taylor, E., Alt, J. et al. (1991). *Proceedings of the Ocean Drilling Program, Scientific Results, 121*. College Station, TX: Ocean Drilling Program.

Winterer, E.L., Ewing, J.I. et al. (1973). *Initial Reports of the Deep Sea Drilling Project, 17.* Washington, DC: U.S. Government Printing Office.

Witts, J.D., Whittle, R.J., Wignall, P.B., Crame, j.A., Francis, J.E., Newton, R.J., & Bowman, V. (2016). Macrofossil evidence for a rapid and severe Cretaceous–Paleogene mass extinction in Antarctica. *Nature Communications, 7*, 11738. doi:10.1038/ncomms11738.

Witts,J.D., Newton, R.J., Mills, B.J.W., Wignall .P.B., Bottrell, S.H., Hall, J.L.O., Francis, J.E. & Crame, J.A. (2018). The impact of the Cretaceous–Paleogene (K–Pg) mass extinction event on the global sulfur cycle: Evidence from Seymour Island, Antarctica. *Geochimica et Cosmochimica Acta*, 230, 17-45. https://doi.org/10.1016/j.gca.2018.02.037

Worzel, J.L., Bryant, W. et al. (1973). *Initial Reports of the Deep Sea Drilling Project, 10.* Washington, DC: U.S. Government Printing Office.

Zachos, J.C., Arthur, M.A., Thunell, R.C., Williams, D.F., & Tappa. E.J. (1985). Stable isotope and trace element geochemistry of carbonate sediments across the Cretaceous/Tertiary boundary at Deep Sea Drilling Project Hole 577, Leg 86. In G.R. Heath, L.H. Burckle, et al., *Initial Reports of the Deep Sea Drilling Project, 86.*Washington DC: U.S. Government Printing Office, 513-532. doi:10.2973/dsdp.proc.86.120.1985

Zachos, J.C., Arthur, M.A., & Dean, W.E. (1989). Geochemical evidence for suppression of pelagic marine productivity at the Cretaceous/Tertiary boundary: *Nature, 337*, 61–64.

Zachos, J.C., Kroon, D., Blum, P. et al. (2004). *Proceedings of the Ocean Drilling Program, Initial Results 208*. College Station, TX, Ocean Drilling Program. doi:10.2973/odp.proc.ir.208.2004

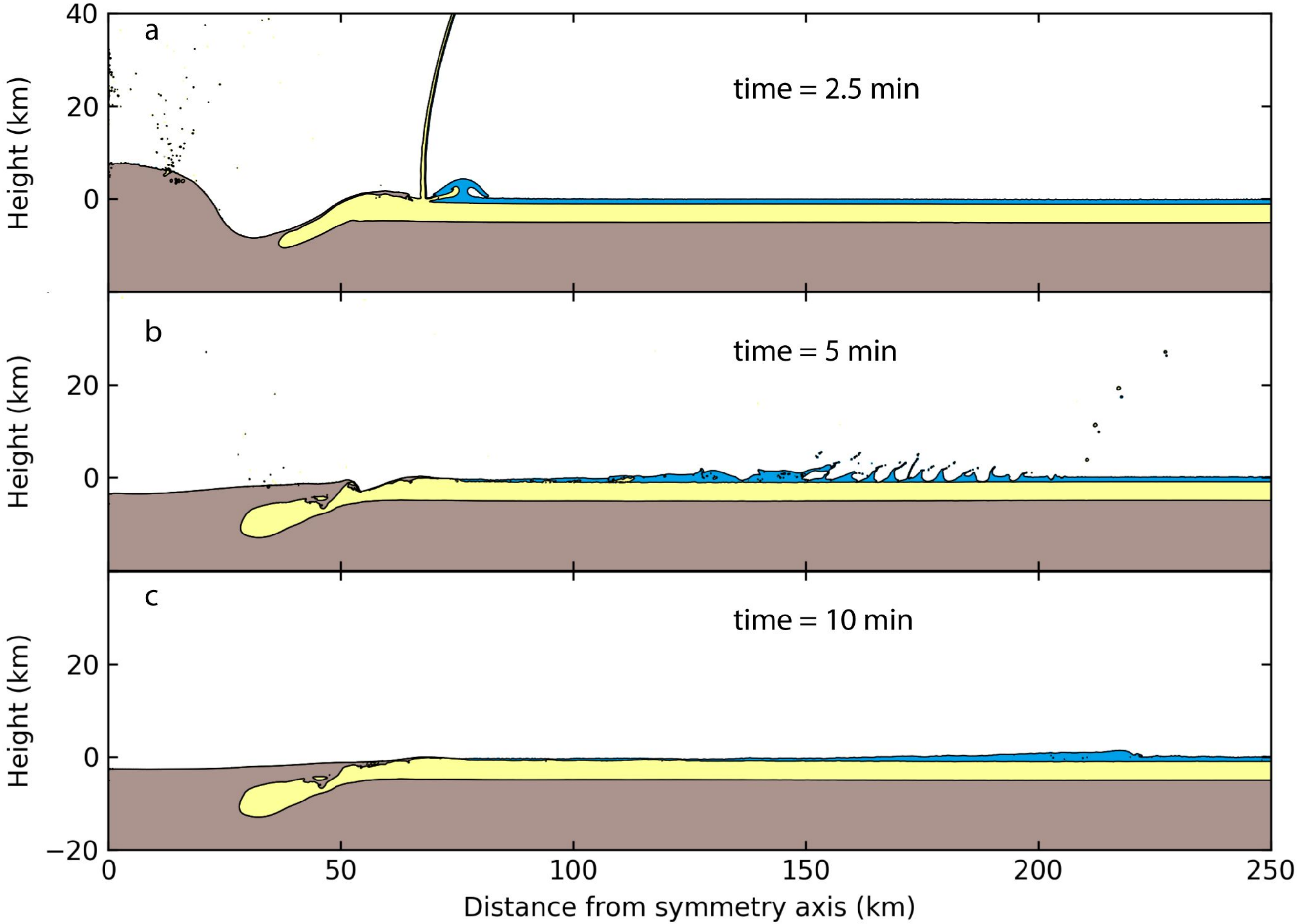

a
time = 2.5 min
b
time = 5 min
c
time = 10 min
Height (km)
Height (km)
Height (km)
40
20
0
20
0
20
0
−20
0
50
100
150
200
250
Distance from symmetry axis (km)

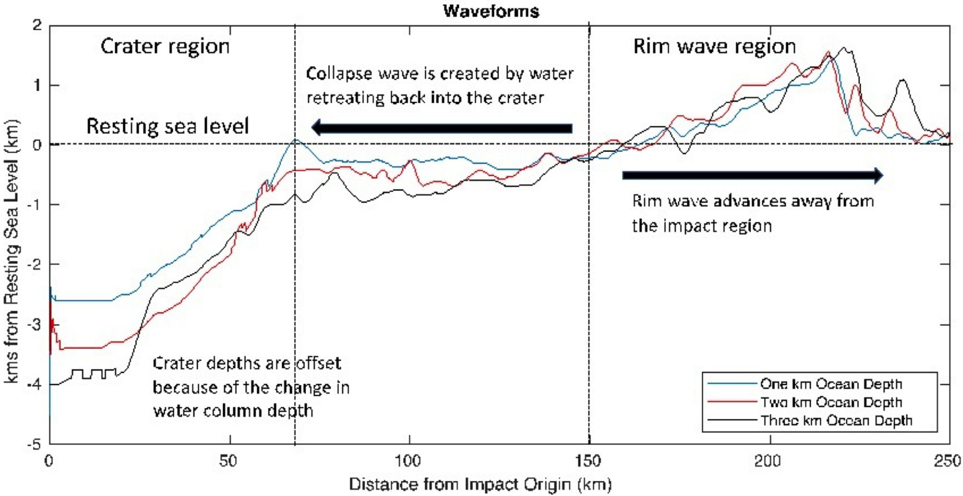

Waveforms
Crater region
Rim wave region
Collapse wave is created by water retreating back into the crater
Resting sea level
Rim wave advances away from the impact region
Crater depths are offset because of the change in water column depth
One km Ocean Depth
Two km Ocean Depth
Three km Ocean Depth
kms from Resting Sea Level (km)
Distance from Impact Origin (km)
2
1
0
-1
-2
-3
-4
-5
0
50
100
150
200
250

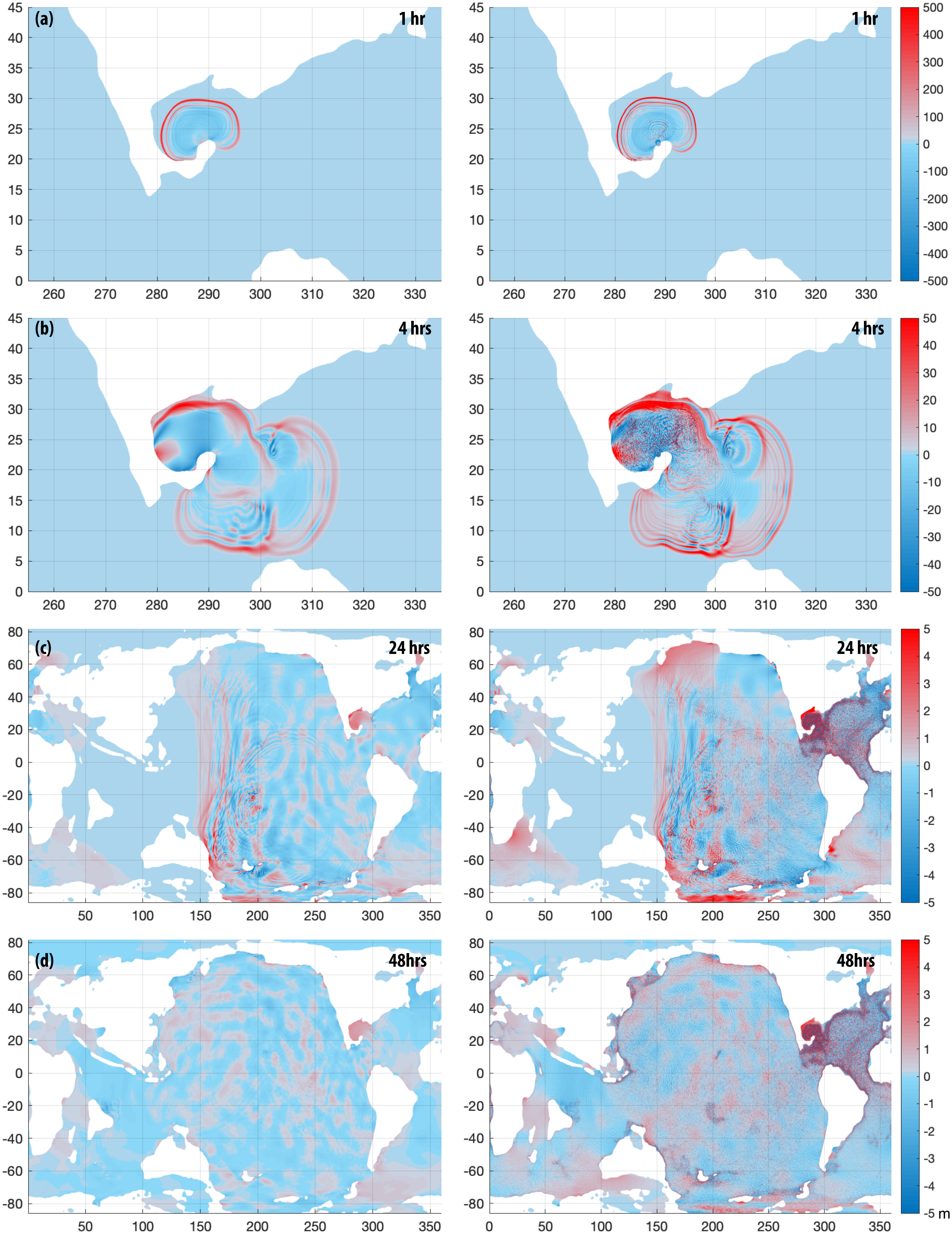

(a)
1 hr
1 hr
(b)
4 hrs
4 hrs
(c)
24 hrs
24 hrs
(d)
48hrs
48hrs
-5 m

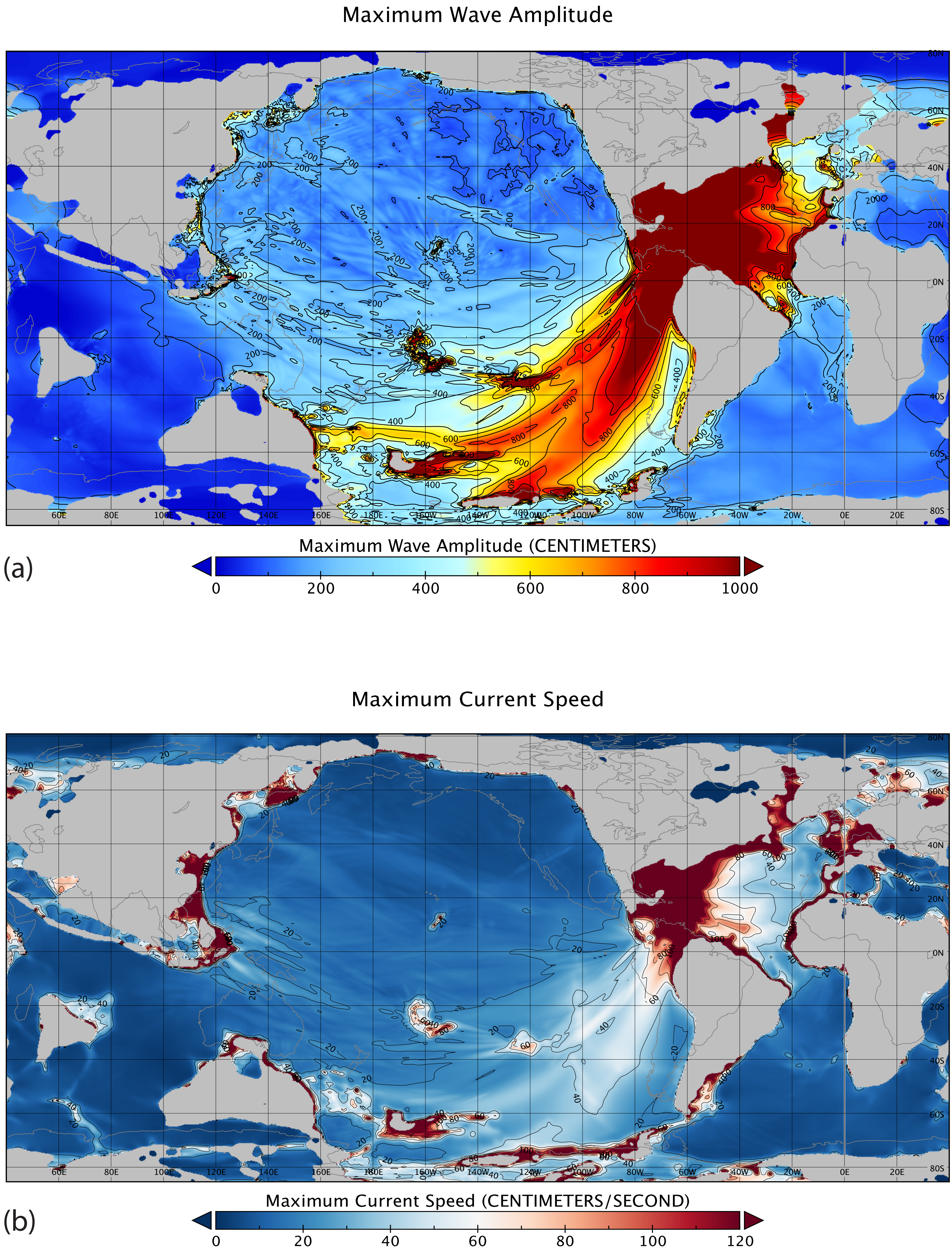
Maximum Wave Amplitude
Maximum Wave Amplitude (CENTIMETERS)
0
200
400
600
800
1000
(a)
Maximum Current Speed
Maximum Current Speed (CENTIMETERS/SECOND)
0
20
40
60
80
100
120
(b)


drill core
outcrop
Complete K/Pg boundary
K/Pg boundary hiatus
Long hiatus
30°
60°
90°
120°
150°
−180°
−150°
−120°
−90°
−60°
−30°
0°
60°
30°
0°
−30°
−60°

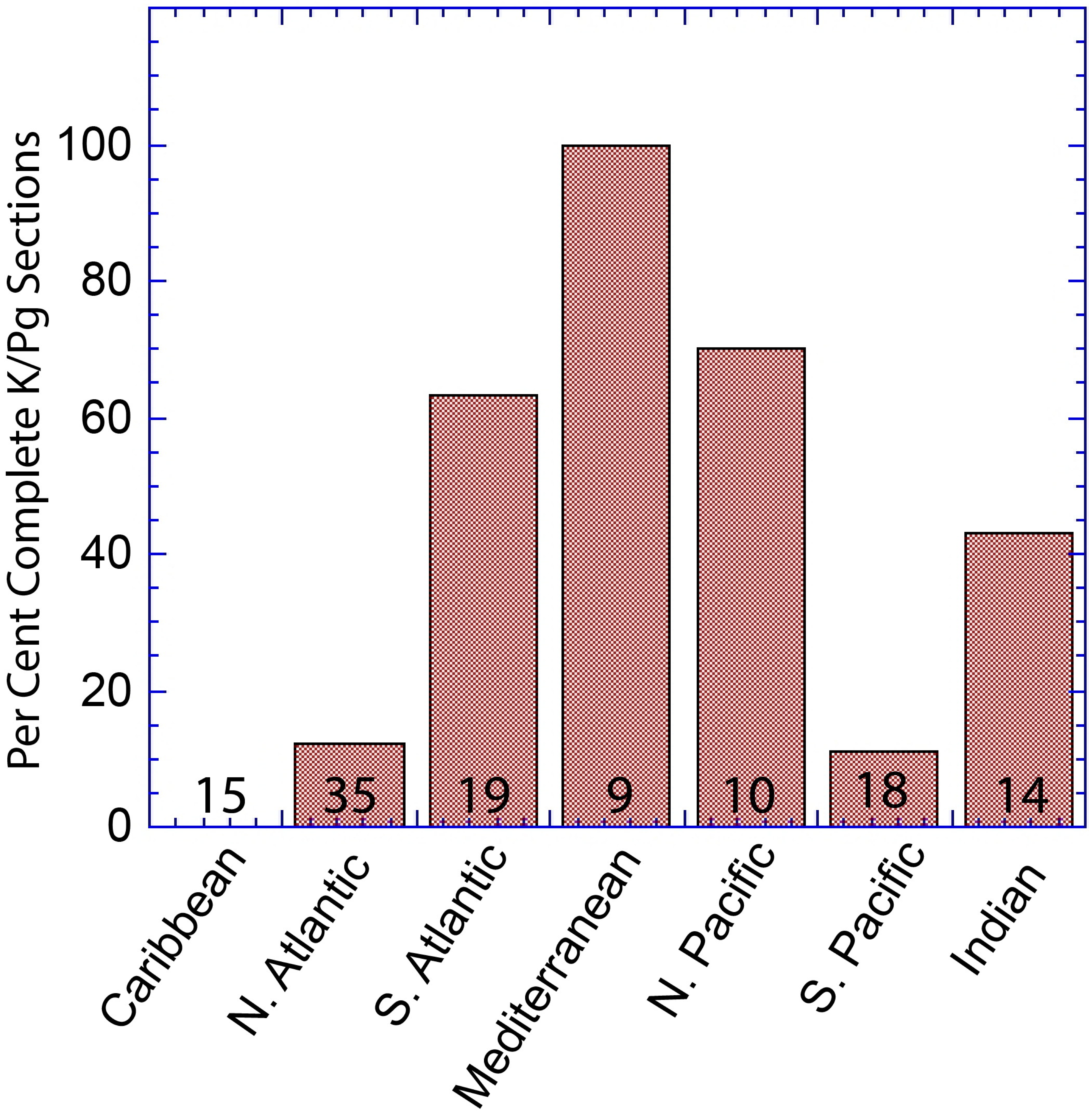

Per Cent Complete K/Pg Sections
0
20
40
60
80
100
15
35
19
9
10
18
14
Caribbean
N. Atlantic
S. Atlantic
Mediterranean
N. Pacific
S. Pacific
Indian